

FLOW IN COLLAPSIBLE TUBES

6.1 Physiological and experimental background*6.1.1 Physiological phenomena*

The main emphasis of the previous four chapters has been on the explanation and prediction of the normal distributions of pressure, velocity and wall shear stress in large arteries. These are the areas in which theoretical fluid mechanics has already made a considerable contribution. In this chapter we turn to an area that has had far less extensive study, although it is medically important and throws up fluid mechanical problems quite as challenging as those examined above. The phenomena we wish to describe are those that occur when the flow of fluid through an elastic tube causes it to collapse, i.e. to suffer a large reduction in cross-sectional area. We saw in § 1.1 that blood vessels (and rubber tubes) are very distensible, and therefore readily experience collapse, when the transmural pressure \hat{p}_{tm} (the difference between the internal and external pressure) is close to zero. This has the consequence that veins above the level of the heart, with the exception of those in the skull, are normally collapsed. The mean flow-rate through a raised venous bed (e.g. in the arm) is, of course, unaltered because the impedance of the whole circulatory bed is primarily determined by the viscoelastic properties of the arteries and by the resistance of the microcirculation; venous calibre is unimportant. Hence the mean blood velocity in the veins is likely to increase when they collapse.

Collapse also occurs in abdominal veins just before they enter the thorax, since abdominal pressure (in a horizontal subject) is normally slightly above atmospheric (about 0.26 kN m^{-2}) and intrathoracic pressure is variable, but normally subatmospheric (by 0.5 kN m^{-2} or more), except during forced expiration. Thus the blood passes through a chamber of high pressure into a chamber of low pressure and the veins tend to collapse just outside the chest. A

similar collapse occurs in veins entering the top of the chest, but since the pressure outside them is atmospheric, the pressure in the chest must be slightly lower before collapse occurs. This collapse has the important consequence that venous return to the heart, and hence the cardiac output, is largely unaffected by the actual value of the pressure in the chest, as long as that is subatmospheric, since it is determined by the end-capillary pressure and by the extent of the collapse, i.e. by the pressure outside the collapsed veins. An increase of intrathoracic pressure above atmospheric does tend to decrease venous return because then there is no collapse and the effective downstream pressure for venous flow is that of the right atrium, i.e. of the chest. (See fig. 6.1(a) and (b); fig. 6.1(a) was adapted from Holt (1969) who gives a fuller discussion.) The tendency of veins to change their cross-section markedly with variations in transmural pressure is exploited normally in the assistance of venous return by intermittent contraction of the skeletal muscle surrounding the veins. It is also exploited clinically, in that rhythmic compression of the legs of a patient who has recently undergone surgery, without changing the average flow-rate, is found to decrease significantly the incidence of deep-vein thrombosis, one of the major causes of post-operative complications. (See Scherer *et al.*, 1975a; Caro *et al.*, 1978, chapter 14.)

Mention should also be made of the vessels in the pulmonary circulation, which is a low-pressure system surrounded by approximately atmospheric pressure in the respiratory airspaces. The normal pressure in pulmonary capillaries and veins is only a fraction of a kN m^{-2} above atmospheric, and any reduction in left atrial pressure or any increase in the air pressure in the lungs can cause collapse of these vessels. Indeed, blood vessels at the top of the lung normally are collapsed in an upright subject because the fall in hydrostatic pressure with height reduces their internal pressure below atmospheric. We should also notice that the airways themselves suffer collapse during forced expiration, with the consequence that at any particular lung volume there is a maximum expiratory flow-rate, which cannot be exceeded however much effort is made: see Clément, van de Woestijne & Pardaens (1973), Lambert & Wilson (1972, 1973), and Dawson & Elliott (1977) for theoretical approaches to this phenomenon.

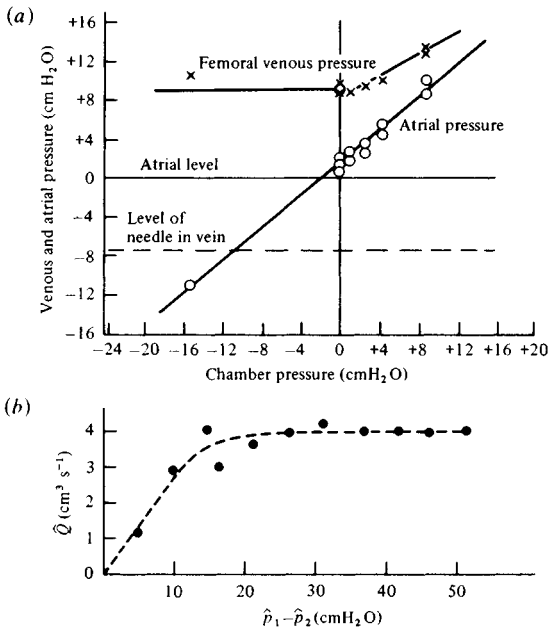


Fig. 6.1. (a) Effect of changing intrathoracic pressure on right atrial and femoral venous pressure in a dog whose trachea is connected to a breathing chamber. Intrathoracic pressure was varied by changing the pressure in the chamber from 20 cmH₂O above atmospheric pressure to 20 cmH₂O below. The hydrostatic level of the needle in the femoral vein was approximately 8 cm below the level of the right atrium. +, above atmospheric pressure; -, below atmospheric pressure. (After Holt, 1969.) (b) Measurements by Brecher (1952) representing the steady flux through the superior vena cava of a dog as a function of the pressure difference $\hat{p}_1 - \hat{p}_2$, where \hat{p}_1 is the pressure in the jugular vein and \hat{p}_2 is the pressure applied to the peripheral end. (After Rubinow & Keller, 1972.)

We saw in § 1.2 that systemic arteries do not normally suffer collapse, but those in a limb can do so when bent in a joint or when compressed by a pressure cuff. The appearance and disappearance of audible Korotkoff sounds, which are presumably a consequence of the collapse, are used as indications of systolic and diastolic arterial blood pressure.

In the next subsection we describe model experiments, performed with rubber tubes, in which the collapse process can be studied more directly than *in vivo*, and note particular phenomena that fluid mechanical theory should be able to explain. We follow

that by discussing some of the theories that have been put forward as explanations of Korotkoff sounds, in an attempt to see what should comprise a complete explanation. The remaining sections of this chapter outline some of the theoretical work that has been done in an attempt to explain both the steady and the unsteady phenomena observed in the model experiments.

6.1.2 *Model experiments*

The standard experiment on collapsible tubes is that depicted in fig. 6.2 and described by Conrad (1969), Holt (1969) and Katz, Chen & Moreno (1969) among others. A segment of flexible tube is supported horizontally between two lengths of rigid tube and is contained in a chamber whose pressure, \hat{p}_c , can be given any chosen value. The upstream and downstream pressures in the rigid tubes, \hat{p}_1 and \hat{p}_2 , can be measured, as can the flow-rate, \hat{Q} , through the system. Fluid is supplied from a reservoir whose height, \hat{H} , above the collapsible segment can be varied, as can the resistances, \hat{R}_1 and \hat{R}_2 , of two variable constrictions upstream and downstream of the region of interest. Thus it is possible to vary conditions upstream, downstream and around the collapsible segment independently.

We describe first the results obtained when the chamber pressure \hat{p}_c and the downstream resistance \hat{R}_2 are held constant, and the flow-rate through the system is varied by varying either \hat{R}_1 or \hat{H} . Fig. 6.3 presents families of graphs of \hat{p}_1 , \hat{p}_2 and $\hat{p}_1 - \hat{p}_2$ against \hat{Q} , each curve representing a different downstream resistance \hat{R}_2 . Fig. 6.4 shows a single curve from a family like that of fig. 6.3(c), together with sketches of the state of collapse of the flexible segment at different points on the curve. There are three distinct sections of this curve, as follows.

(I) The downstream pressure \hat{p}_2 increases monotonically with \hat{Q} , (fig. 6.3(b)) by virtue of the fixed downstream constriction (these curves are not linear, as they would be for a constant resistance ($\hat{p}_2 = \hat{R}_2 \hat{Q}$), but are of the form

$$\hat{p}_2 = k_1 \hat{Q}^2 + k_2 \quad (6.1)$$

since the constriction was a sharp orifice). Therefore, when the flow-rate is sufficiently large, \hat{p}_2 can exceed \hat{p}_c by an arbitrary amount, and so the pressure everywhere in the collapsible segment

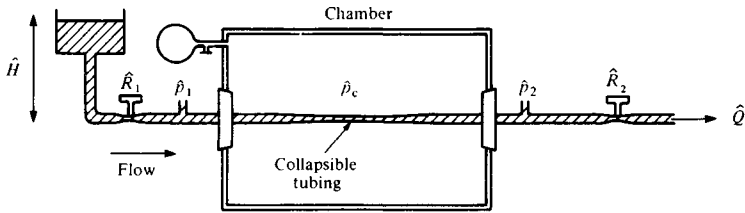


Fig. 6.2. Experimental arrangement for studying flow in a collapsible tube.

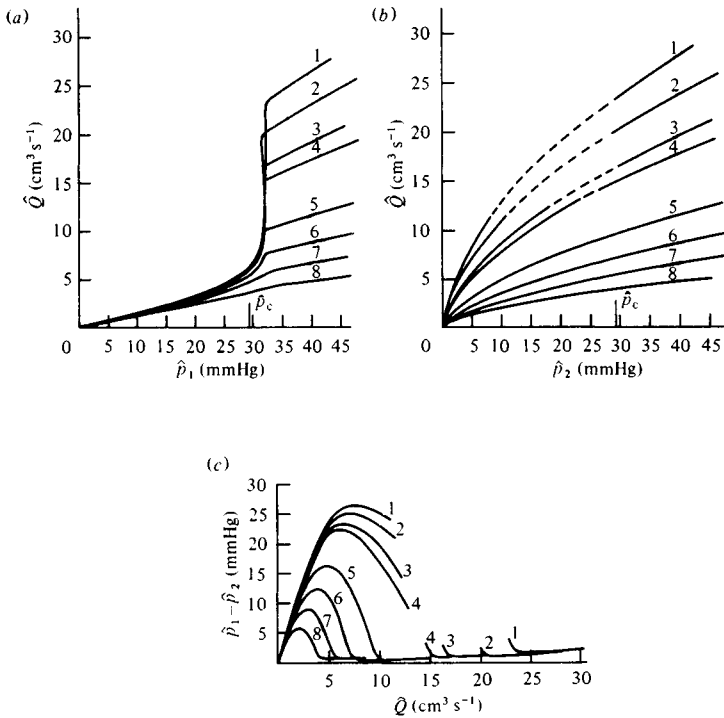


Fig. 6.3. (a) \hat{p}_1 as a function of \hat{Q} for constant external pressure ($\hat{p}_c = 29.5$ mmHg) and different settings of the downstream resistance. Curves correspond to different values of k_1 in (6.1) measured in $\text{mmHg} (\text{cm}^3 \text{s}^{-1})^{-2}$: 1, 0.05; 2, 0.07; 3, 0.10; 4, 0.12; 5, 0.27; 6, 0.45; 7, 0.9; 8, 4.0. (b) \hat{p}_2 as a function of \hat{Q} . (c) Pressure drop $\hat{p}_1 - \hat{p}_2$ as a function of \hat{Q} ; breaks in the curves represent regions of oscillation. (After Conrad, 1969.)

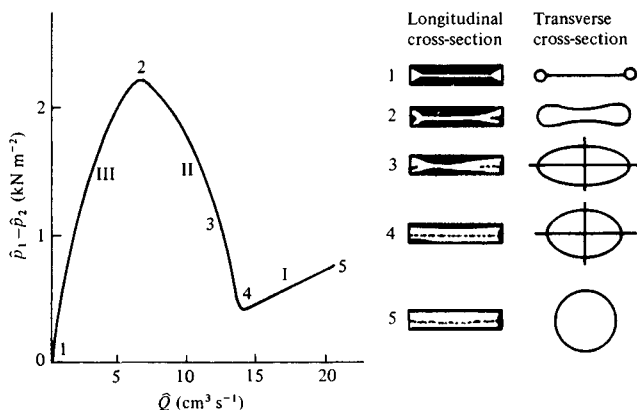


Fig. 6.4. Pressure drop across the collapsible segment as a function of flow-rate for fixed downstream resistance and external pressure. Longitudinal and transverse cross-sections at various flow-rates are also shown: 1, zero flow; 2, small flow; 3, 4, larger flows; 5, flow so large that tube has become circular. Flow is from right to left. (After Conrad, 1969)

exceeds \hat{p}_c by at least as much. Hence, according to the relation between transmural pressure and cross-sectional area (fig. 1.10(a)), the cross-section of the segment is everywhere circular and is very stiff, so that the flow within it is everywhere Poiseuille flow. Thus $\hat{p}_1 - \hat{p}_2$ is proportional to \hat{Q} , with an almost constant resistance.

(II) When \hat{Q} is reduced below a certain critical value, the downstream pressure \hat{p}_2 becomes as small as, or smaller than, the chamber pressure \hat{p}_c , so that the cross-section of the collapsible segment begins to change shape and to collapse towards the downstream end (again according to fig. 1.10(a)). As the transmural pressure falls further, the cross-sectional area at the downstream end falls rapidly, because of the large distensibility; the collapse of the flexible segment also extends further upstream. This means that the resistance to flow rises rapidly, both because of the increase in the viscous resistance of a narrowed tube and because of the energy dissipation in the separated jet that must emerge where the tube has to widen out again as it joins the downstream rigid segment (this jet will in many cases be turbulent). Thus the pressure drop required to maintain the (gradually falling) flow-rate also rises dramatically.

(III) Finally, when the whole segment is collapsed ($\hat{p}_1 < \hat{p}_c$), its cross-section has a rather rigid dumb-bell configuration, and, as the flow-rate is reduced still further, no further change in cross-section occurs, the resistance once more becoming constant, at a value 10–100 times higher than before collapse.

If, instead of varying the upstream conditions, we vary the downstream resistance \hat{R}_2 , so that \hat{p}_2 is varied independently of \hat{p}_1 , then when \hat{p}_2 exceeds \hat{p}_c by a sufficient amount, the flow-rate is again proportional to $\hat{p}_1 - \hat{p}_2$. However, when \hat{p}_2 falls below \hat{p}_c , collapse begins; because \hat{p}_1 remains high, this collapse does not extend throughout the flexible segment, and a fixed degree of collapse results. Further reduction in \hat{p}_2 has no effect on the flow-rate, as shown in fig. 6.5 (see fig. 6.1 for evidence of this phenomenon *in vivo*). Note the overshoot of flow-rate in fig. 6.5(a), reflecting the progression of the collapse process to its final state as \hat{p}_2 falls below \hat{p}_c . Physiologists have for many years used segments of collapsible tube in this way as part of the apparatus for perfusing different parts of the circulatory system at a constant flow-rate, independent of downstream pressure. The device is known as a 'Starling resistor', having been introduced by Knowlton & Starling (1912).

Varying \hat{p}_c independently of \hat{p}_1 and \hat{p}_2 also has a predictable effect: if $\hat{p}_c < \hat{p}_2$, there is no collapse and \hat{Q} is independent of \hat{p}_c ; however, as \hat{p}_c rises above \hat{p}_2 it is $\hat{p}_1 - \hat{p}_c$ not $\hat{p}_1 - \hat{p}_2$ that governs the flow-rate.

In most experiments on collapsible tubes, an important phenomenon is observed when the tube is partially collapsed (section II of fig. 6.4). That is that self-excited oscillations, in area, flow-rate and \hat{p}_2 , are found to develop during this phase, even when the upstream reservoir, the upstream and downstream resistances, and the chamber pressure are held fixed. Both Conrad (1969) and Katz *et al.* (1969) report that, when the flow-rate is varied by adjustment of upstream conditions, oscillations occur only for sufficiently small values of the downstream resistance \hat{R}_2 (or the constant k_1 in (6.1)); the breaks in the curves in figs. 6.3(b) and (c) indicate that oscillations were taking place. Some of Katz *et al.*'s results indicate that when \hat{R}_2 is such that no oscillations take place for a given value of \hat{p}_c , then increasing \hat{p}_c (and hence increasing the

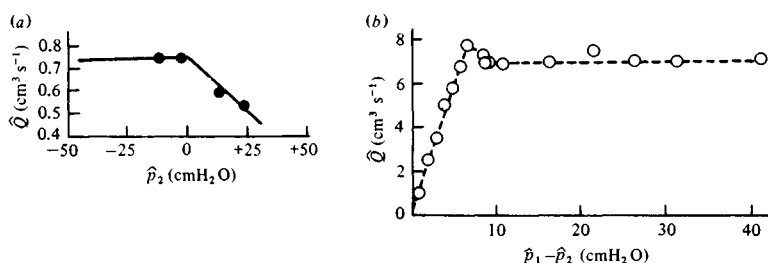


Fig. 6.5. (a) Effect on flow-rate of changing \hat{p}_2 , keeping \hat{p}_1 and \hat{p}_c constant. (After Holt, 1969.) (b) The same, from measurements of Brecher (1952). (After Rubinow & Keller, 1972.)

extent of collapse) does not generate oscillations. Conrad (1969) showed one set of results indicating that the frequency of the oscillations increases as the flow-rate decreases through section II of fig. 6.4. In his case the frequency range was 0.6 Hz to 1.7 Hz (his tubes had an undisturbed diameter, d , of 1.27 cm). However, J. M. Fitz-Gerald (private communication) and Conrad, Cohen & McQueen (1978) have reported a much wider range of frequencies, depending on the values of \hat{R}_1 , \hat{R}_2 , \hat{p}_c and d and on the precise elastic properties of the tube. This is borne out by the experience of Ur & Gordon (1970) who performed experiments using both rubber tubes and excised segments of artery (diameter 0.4 cm) and who reported frequencies in the range 12 Hz to 50 Hz. Their experiments are described further in § 6.1.3.

The ultimate aim of theoretical studies is to explain the above phenomena accompanying flow in collapsible tubes; the theoretical description of the self-excited oscillations is a particularly challenging problem. In §§ 6.2–6.3 we introduce various avenues of approach that are currently proving fruitful, although in no case is the work yet complete. First, however, we look more closely at the particular phenomenon of Korotkoff sounds, and discuss the various mechanisms that have been put forward to explain them.

6.1.3 Mechanisms of Korotkoff sounds

The phenomenon of Korotkoff sounds was described in § 1.2; they are heard when a cuff is inflated round a limb until the pressure exceeds systolic arterial pressure and the arteries are occluded, and

then the cuff pressure is gradually reduced. The sounds are characterised by a sharp clicking noise as cuff pressure, \hat{p}_c , falls below systolic arterial pressure. This becomes louder, and may be followed by a brief murmur as \hat{p}_c is reduced further; subsequently the sound becomes muffled, and it finally disappears when cuff pressure is close to diastolic pressure. The high-frequency (60–180 Hz) content of the sounds at different stages of cuff deflation was shown in fig. 1.27.

Various apparently different mechanisms have been proposed to explain the sounds, but one factor that they all share is the importance of the collapsibility of the artery wall when subjected to external compression. When the cuff pressure is significantly greater than diastolic, but less than systolic, pressure, the artery is occluded for most of the cycle. When the pulse arrives the artery is forced open, subsequently to close again as the pulse pressure falls. Gonzalez (1974) recorded the sounds accompanying this process in a human brachial artery, both over the cuff and some way downstream, and reported a single sharp spike on the recording (the click lasting 0.02–0.04 s), followed by a lower-amplitude noisy murmur, lasting about 0.1 s, in most subjects. The period of the cardiac cycle was about 1.0 s. He associated the click with a steep pressure wave (a 'shock': § 2.1.4) formed as blood is forced through the opening constriction, and terminated as the constriction closes again. The time lapse between the sounds heard at the cuff and at a known distance downstream was consistent with wavefront propagation at the speed predicted by the theory of chapter 2. Gonzalez did not report coherent oscillations as the artery closed again towards the end of systole. Nor did he record frequency spectra, but the nature of the signal, backed up by flow visualisation in models, suggested that the murmur, which persists into diastole, is associated with turbulence generated by the jet-like flow through the constriction in systole. When the cuff pressure is close to systolic, the click is heard but not the murmur, which he attributed to insufficient time for turbulence to be generated in the jet. When cuff pressure is only a few hundred N m^{-2} above diastolic pressure, the clicking becomes muffled, because, according to this author, the artery does not collapse completely. At an even lower pressure the audible sound disappears altogether, but the precise value of cuff pressure at which

this occurs depends on the characteristics of the sound-recording equipment, and may still be above diastolic pressure. The qualitative conclusions of this author seem plausible, but it is a pity that he did not record frequency spectra for comparison with the measurements of other workers (e.g. McCutcheon & Rushmer, 1967), and with the known characteristics of intermittent turbulent flow through constrictions (Young & Tsai, 1973*b*).

More insight can be gained from the observations of Ur & Gordon (1970), who recorded Korotkoff sounds in the brachial artery of a dog. They do not present such a recording, but they do show direct upstream and downstream pressure measurements taken in the same animal, after death, when the artery was connected upstream to a perfusion system in order to provide a known pressure head. These measurements are compared with those made in isolated limbs, and in excised arteries and rubber tubes supported as in fig. 6.2. In each of these preparations the authors performed three different manoeuvres, and in each case all preparations gave qualitatively similar results. One was to keep upstream and cuff pressures steady, as in the experiments of Conrad (1969) and others, and in this case continuous self-excited oscillations were recorded for a wide range of upstream and cuff pressures, as in the experiments already described.

The second manoeuvre was to reduce the upstream pressure, while keeping cuff pressure constant; this manoeuvre is intended to simulate the fall in arterial pressure after peak systole, but does not model the early part of systole in which the arterial pressure rises and (if cuff pressure exceeds diastolic pressure) forces the artery open. The pressure recordings from one such experiment (in an excised artery) are shown in fig. 6.6(*a*), together with the sound recorded through a stethoscope. It can be seen that, as the upstream pressure falls past the value of the cuff pressure, oscillations of a fixed frequency are generated in downstream pressure and in sound recorded (oscillations in area were simultaneously observed). Aurally, the sound resembles the click of Korotkoff sounds, but these measurements differ from those of Gonzalez by virtue of the oscillations. The two sets of experiments can be reconciled, however, if account is taken of the *rate* at which upstream pressure

is reduced. Ur & Gordon recorded no oscillations and no clicking sound (cf. fig. 6.6(b)) when the upstream pressure reduction in the models took place very rapidly and lasted for less than 0.25 s; occlusion of the artery also took place rapidly, as in the in-vivo experiments of Gonzalez (1974). Admittedly the diastolic pressure fall *in vivo* lasts for almost three-quarters of the cycle, or about 0.7 s in man, which exceeds the critical value of 0.25 s in Ur & Gordon's experiments. However, Ur & Gordon did not report the critical reduction time in the isolated limb or in the dead dog, although they did report an abbreviation of the time over which oscillations could be heard, in the former, as the pressure was reduced more rapidly. Since the elastic properties of an artery tethered to its surrounding tissue are different from its properties when excised, even if stretched to its in-vivo length, a change in the critical reduction time would not be surprising (tethering also, no doubt, accounts for the fact that the oscillation frequency in the dog's brachial artery is much less *in vivo* (4–8 Hz) than *in vitro* (12–50 Hz)). In summary, then, collapse of the artery in diastole is likely to be accompanied by a burst of self-excited oscillations as long as the arterial pressure does not fall too rapidly. The evidence of Gonzalez is that the oscillations are absent *in vivo*, but their prevalence in Ur & Gordon's experiments suggests that they could occur, even *in vivo*, if circumstances were suitable.

The third manoeuvre performed by Ur & Gordon was intended to simulate systole by raising cuff pressure until the artery was occluded, and then allowing it to fall while holding upstream conditions constant. However, because the fluid level in their upstream reservoir was not kept constant, the upstream pressure also fell once outflow had begun, and the simulation was not exact. Nevertheless, figs. 6.6(b) and (c) show that the results were very similar to the 'diastolic' results, in that oscillations of given frequency occurred during the pressure fall as long as the rate of fall was not too rapid.

The fact that Ur & Gordon reported no sounds during the experiments with rapid pressure reductions, while Gonzalez (1974) still reported a click *in vivo*, is presumably associated with the fact that Ur & Gordon modelled only diastole or systole, not a complete beat. Thus the brief, steep pressure pulse formed *in vivo* is likely to

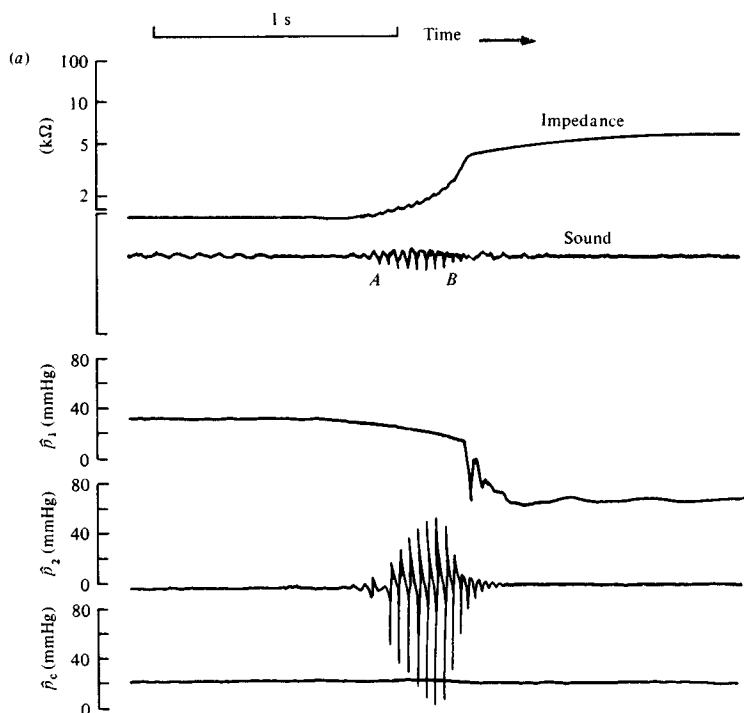
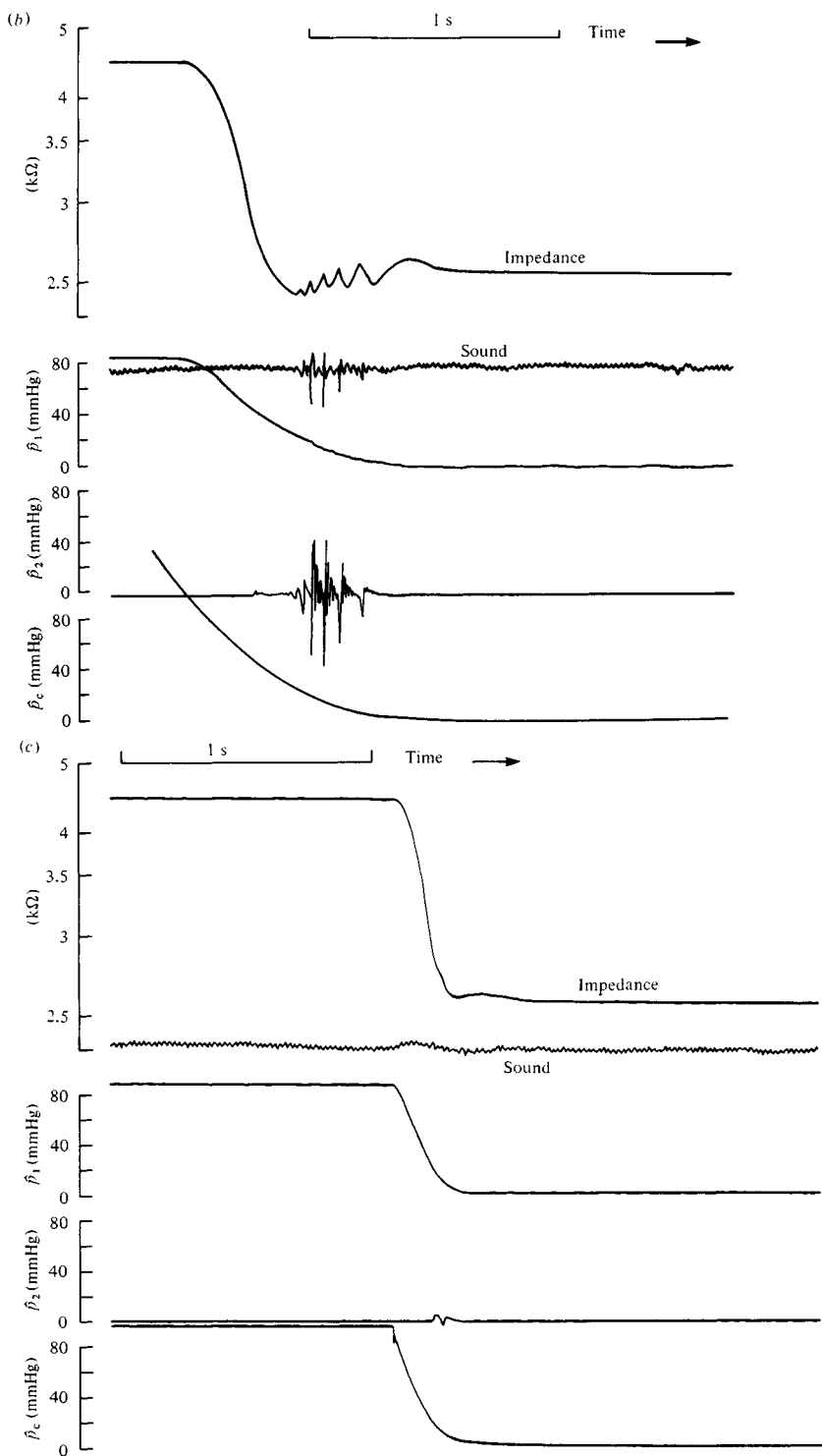


Fig. 6.6. (a) Oscillation and sound production in an excised segment of artery. The uppermost trace records the electrical impedance of a section of the tube including the collapsed region; this is related (but not directly proportional) to the cross-sectional area at the narrowest point. A rapid reduction in reservoir pressure, simulating diastole, produces a click consisting of a short burst of oscillation lasting about 300 ms. (b) Production of a click in the model by rapid reduction of chamber pressure. (c) More rapid reduction of the chamber pressure causes the tube to open in a very short time without significant oscillation or sound production. (After Ur & Gordon, 1970.)

be absent. Further points to be noted from Ur & Gordon's experiments are:

- (a) High-speed cine-photography showed that waves were propagated both upstream and downstream from the oscillating constriction; these are presumably pressure waves as analysed in chapter 2.



- (b) If the upstream pressure is varied very slowly, the frequency of the oscillations also varies slowly, being 2–3 times as great at low values of the pressure difference $\hat{p}_1 - \hat{p}_c$ than at high values; this is consistent with the observations of Conrad (1969).

Ur & Gordon did not report the ‘murmurs’ which follow the ‘clicks’ in both McCutcheon & Rushmer’s (1967) and Gonzalez’s (1974) recordings of real Korotkoff sounds. However, close examination of one of their recordings taken with an expanded time-scale (fig. 6.7) reveals the presence of irregular, high-frequency, low-amplitude fluctuations superimposed on the basic oscillations. They also reported similar fluctuations in steady flow past a fixed constriction, when turbulence is to be anticipated. Furthermore, the canine artery used by Ur & Gordon had a diameter of about 0.4 cm, which is smaller than the human brachial artery (about 0.6 cm) so that the Reynolds number downstream of the constriction is also likely to be smaller (although Ur & Gordon did not quote velocity). That would mean that the intensity of any turbulence produced would be less than in Gonzalez’s subjects. Thus there seems no reason to doubt the conclusion of Gonzalez that the murmur originates in the turbulent jet downstream of the constriction. Whether or not it occurs depends both on the Reynolds number in the artery and on the degree of constriction. In steady flow this follows from the fact that, as long as there is flow separation, turbulence occurs if the Reynolds number *at the constriction* exceeds a value that depends on the geometry of the constriction, but that can be as low as 500–600. Its persistence downstream, however, depends on the Reynolds number in the undisturbed tube. In unsteady flow, the occurrence of turbulence depends on the amount of time available for the growth of small disturbances (cf. § 5.3), and is complicated (Young & Tsai, 1973a).

The above discussion has linked Korotkoff sounds with particular events in the flow of blood through a collapsing artery, but has not given a fluid dynamical explanation of those events. One such ‘explanation’ has been provided by Anliker & Raman (1966), who proposed a model to predict that value of cuff pressure, above diastolic, at which the circular configuration of the artery wall first becomes unstable. The artery wall is then expected to buckle and

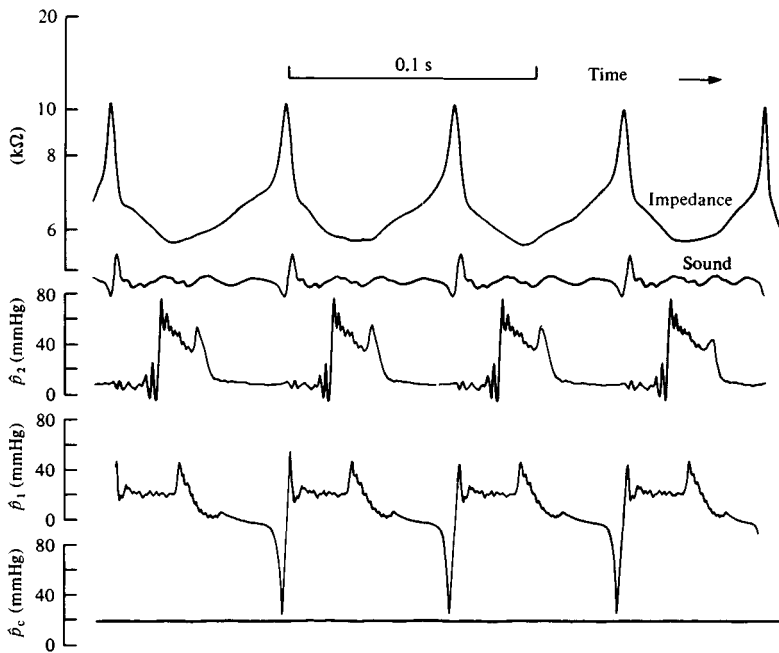


Fig. 6.7. Detailed recording of oscillation in a segment of latex tube. (After Ur & Gordon, 1970.)

generate sounds, as long as the growth-rate of the growing disturbances is sufficiently rapid for the disturbances to be observable (i.e. audible) before the arterial pressure rises again to a value at which the circular configuration is stable. The stability analysis is another example of Flügge's shell theory (cf. Shayo & Ellen (1974), discussed in § 5.3), and since Anliker & Raman ignored any effect of blood flow, the presence of blood in the artery has no effect on the buckling criterion, its inertia serving merely to determine growth-rates. The analysis predicts stability for a brachial artery, so that Korotkoff sounds must disappear, for cuff pressures less than 800 N m^{-2} (6 mmHg) above diastolic. A better prediction might be made by combining this theory with that of Shayo & Ellen (1974), in which the blood flow itself is a destabilising influence.

The trouble with such stability analyses is that they treat the blood vessel wall as homogeneous and isotropic, with no stresses in the undisturbed configuration, whereas the real artery is much more

complex (§ 1.1). A theory in which these assumptions were relaxed would be extremely complicated. Furthermore, the theory is linear, so it can describe what happens only when the deformations remain quite small, and cannot describe the large changes in cross-section that take place during collapse. In order to make a start on the analysis of the dynamics of collapse and oscillation, therefore, we beg the question posed by elasticity theory, and assume *a priori* that the average transmural pressure across a cross-section of the vessel at any time is related to the local cross-sectional area through a given single-valued function such as one of those presented in fig. 1.10(a). This is very crude, but enables us in the next three sections to concentrate on fluid dynamical aspects of flow and oscillations in collapsible tubes.

6.2 Viscous flow in slowly varying collapsible tubes

In all the model experiments reported above, the Reynolds number of the flow was large, and it is unlikely that the direct action of viscosity was important in most of the phenomena, especially the oscillations whose period is normally much smaller than the time for viscous diffusion across the tube. Nevertheless, although none of the experiments has looked for it, there must exist, in a given experiment, a critical value of the Reynolds number below which oscillations cannot occur; this critical value should be predictable. Furthermore, there are many medium-sized or small veins and pulmonary vessels in which the Reynolds number is less than (say) 10 and that experience compressive transmural pressures. Indeed, observation of pulmonary capillaries shows that it is these smaller vessels that are normally closed at the top of the lung in a resting subject (West *et al.*, 1969). It would be of interest to see if the phenomena reported above for steady flow in large collapsible tubes are still expected to occur in smaller ones.

Work on unsteady viscous flow in collapsible tubes is still at an early stage, so this section is largely devoted to an analysis of steady (and hence also quasi-steady) flow in a finite segment of such a tube at Reynolds numbers around 1 or below. The work is taken from the paper by Wild, Pedley & Riley (1977). The analysis is based on lubrication theory and therefore requires that the cross-sectional

area vary slowly with longitudinal distance. The effect of inertia is analysed as a perturbation to the basic lubrication theory solution; it is important to include it because it is not negligible in any of the (large-Reynolds-number) experiments, and without inertia the self-excited oscillations cannot develop.

The basic solution was first given, and applied to tubes of circular cross-section, by Rubinow & Keller (1972). They showed that the flow-rate, \hat{Q} , and the local pressure gradient, $d\hat{p}/d\hat{x}$, are related by an equation of the form

$$\hat{Q} = -\sigma d\hat{p}/d\hat{x}, \quad (6.2)$$

where σ is the conductivity, which depends on cross-sectional area (as deduced from lubrication theory) and hence, from data such as that of fig. 1.10(a), on transmural pressure, \hat{p}_{tm} . Now $\hat{p}_{tm} = \hat{p} - \hat{p}_c$, where \hat{p} is the internal pressure and \hat{p}_c the external (assumed constant), and \hat{Q} is independent of \hat{x} . Thus if \hat{L} is the distance between the upstream station, where $\hat{p} = \hat{p}_1$, and the downstream station, where $\hat{p} = \hat{p}_2$, integration of (6.2) gives

$$\hat{Q} = \frac{1}{\hat{L}} \int_{\hat{p}_2}^{\hat{p}_1} \sigma(\hat{p} - \hat{p}_c) d\hat{p}. \quad (6.3)$$

If $\hat{p}_2 > \hat{p}_c$, σ will be fairly large and more or less independent of \hat{p} (because the distensibility is small), so \hat{Q} will be approximately proportional to $\hat{p}_1 - \hat{p}_2$. On the other hand, if $\hat{p}_2 < \hat{p}_c$, σ will be very small for values of \hat{p} less than about \hat{p}_c , and (6.3) can be approximately replaced by

$$\hat{Q} \approx \frac{1}{\hat{L}} \int_{\hat{p}_c}^{\hat{p}_1} \sigma(\hat{p} - \hat{p}_c) d\hat{p},$$

which is independent of \hat{p}_2 . This is one explanation of the steady experimental results described above.

Wild *et al.* (1977) extended the work of Rubinow & Keller (1972) in four ways. First, they considered tubes of elliptic cross-section, in order more accurately to model their collapse. This model is incorrect when the cross-section becomes dumb-bell shaped and its area very small, but the measured pressure-area relation (fig. 1.10(a)) is rather uncertain then anyway, and a better model would not make the predictions of conductance (which is very low in these

circumstances) more accurate. (Flaherty *et al.* (1972*a*) computed the shape and conductance σ of a buckled cylindrical tube, linearly elastic and uniform along its length.) Secondly, they included to first order the effects of inertia, as was done for rigid circular tubes by Manton (1971) as a perturbation to lubrication theory, and by Lee & Fung (1970) numerically. Hall (1974) also extended lubrication theory by considering unsteady flow in a slowly varying rigid tube of small eccentricity when a pulsatile pressure difference is applied across its ends. Thirdly, Wild *et al.* did not restrict attention to uniform external pressure \hat{p}_c , but calculated the variation in internal pressure, fluid velocity and tube cross-sectional area when the external pressure varied along the tube, in particular when it resembled that applied by a cuff of finite length (see fig. 6.12). Fourthly, previous calculations had not covered the experiment described above in which the downstream resistance is held constant. Our results do extend to this case, and, in fact, they are found to predict multiple-valued $\hat{Q}-\Delta\hat{p}$ curves like that of fig. 6.4. As in all the quoted work, blood was taken to be a homogeneous and Newtonian fluid, which is a good approximation in vessels of diameter greater than 100 μm , in which the shear-rate exceeds 100 s^{-1} (see § 1.1). An outline of the analysis and the results is given below.

6.2.1 Lubrication theory and the effect of inertia

In steady conditions the shape of the tube does not change with time, and the relation between local pressure gradient and flow in an arbitrary slowly varying elliptical tube can be calculated independently of the pressure–area relation.

We consider steady, viscous incompressible flow through a slowly varying elliptical tube of length L , defined in Cartesian coordinates (Lx, a_0y, a_0z) by

$$y^2/a^2(x) + z^2/b^2(x) = 1 \quad 0 \leq x \leq 1, \quad (6.4)$$

where a_0 is a characteristic tube radius, and a_0a, a_0b are the semi-major and semi-minor axes of the elliptical cross-section. The use of lubrication theory requires that

$$\varepsilon = a_0/\hat{L} \ll 1, \quad (6.5)$$

while the Reynolds number

$$Re = U_0 a_0 / \nu$$

remains $O(1)$ as $\varepsilon \rightarrow 0$; U_0 is a scale for the axial velocity component. The velocity field $\hat{\mathbf{u}}$ is scaled so that each dimensionless component is $O(1)$, and is taken to be

$$\hat{\mathbf{u}} = U_0(u, \varepsilon v, \varepsilon w)$$

with pressure

$$\hat{p} = (\rho U_0^2 / \varepsilon Re) p. \quad (6.6)$$

It is convenient to work in a coordinate system in which the tube cross-section does not vary with x . Accordingly we introduce new transverse coordinates

$$\eta = y/a(x), \quad \zeta = z/b(x),$$

so that (6.4) becomes

$$\eta^2 + \zeta^2 = 1 \quad 0 \leq x \leq 1. \quad (6.7)$$

The full equations of motion are

Continuity

$$Du + (1/a)v_\eta + (1/b)w_\zeta = 0, \quad (6.8)$$

x -momentum

$$\begin{aligned} \varepsilon Re [u Du + (v/a)u_\eta + (w/b)u_\zeta] \\ = -Dp + (1/a^2)u_{\eta\eta} + (1/b^2)u_{\zeta\zeta} + \varepsilon^2 D^2 u, \end{aligned} \quad (6.9)$$

y -momentum

$$\begin{aligned} \varepsilon Re [u Dv + (v/a)v_\eta + (w/b)v_\zeta] \\ = -(1/\varepsilon^2 a)p_\eta + (1/a^2)v_{\eta\eta} + (1/b^2)v_{\zeta\zeta} + \varepsilon^2 D^2 v, \end{aligned} \quad (6.10)$$

z -momentum

$$\begin{aligned} \varepsilon Re [u Dw + (v/a)w_\eta + (w/b)w_\zeta] \\ = -(1/\varepsilon^2 b)p_\zeta + (1/a^2)w_{\eta\eta} + (1/b^2)w_{\zeta\zeta} + \varepsilon^2 D^2 w, \end{aligned} \quad (6.11)$$

where

$$D = \partial/\partial x - (a'/a)\eta \partial/\partial \eta - (b'/b)\zeta \partial/\partial \zeta,$$

and ' means d/dx . The boundary conditions are simply $u = v = w = 0$ on the wall (6.7).

We solve the problem as a power series in ε , on the assumption that $R = O(1)$. Thus we take

$$u = u_0 + \varepsilon u_1 + \varepsilon^2 u_2 + \dots$$

with similar expressions for v , w and p . The leading terms in (6.10) and (6.11) show that p_0 is a function only of x , and the leading term of (6.9) (the equation for unidirectional motion) gives

$$u_0(x, \eta, \zeta) = [a^2 b^2 / 2(a^2 + b^2)] G_0(x) (1 - \eta^2 - \zeta^2),$$

where

$$G_0(x) = -dp_0/dx.$$

This is the elliptical-tube version of Poiseuille flow. For given functions $a(x)$ and $b(x)$, G_0 is determined by the condition that the volume flow-rate is independent of x . If U_0 is defined as the average velocity of the flow when the tube cross-section is a circle of radius a_0 , and if volume flow-rate is non-dimensionalised with respect to $a_0^2 U_0$, we have

$$Q = \int \int_{\text{cross-section}} uab \, d\eta \, d\zeta = \pi.$$

Hence

$$G_0 = 4(a^2 + b^2)/a^3 b^3 \quad (6.12)$$

and

$$u_0 = (2/ab)(1 - \eta^2 - \zeta^2).$$

This is the basic lubrication theory solution, leading to a value for the conductance σ , from (6.2), of

$$\sigma = (\pi/4\mu)[\hat{a}^3 \hat{b}^3 / (\hat{a}^2 + \hat{b}^2)]. \quad (6.13)$$

In order to determine the next approximation to u and p it is necessary to calculate the leading terms of the expansions for the secondary velocities, v_0 and w_0 . Equations (6.10) and (6.11) require that these quantities satisfy

$$\frac{1}{a} v_{0\eta\eta\zeta} + \frac{a}{b^2} v_{0\zeta\zeta\zeta} = \frac{b}{a^2} w_{0\eta\eta\eta} + \frac{1}{b} w_{0\eta\zeta\zeta},$$

and (6.8) and (6.13) imply

$$\frac{1}{a} v_{0\eta} + \frac{1}{b} w_{0\zeta} = \frac{2(ab)'}{a^2 b^2} (1 - \eta^2 - \zeta^2) - \frac{4}{ab} \left(\frac{a'}{a} \eta^2 + \frac{b'}{b} \zeta^2 \right).$$

The solution that satisfies the boundary conditions is

$$v_0 = (2a'/ab)\eta(1 - \eta^2 - \zeta^2), \quad w_0 = (2b'/ab)\zeta(1 - \eta^2 - \zeta^2). \quad (6.14)$$

We note that the streamlines of these secondary motions are the same as those of stagnation point flow as long as a' and b' have opposite signs, since

$$\frac{v_0}{w_0} = \frac{a'\eta}{b'\zeta} = \frac{ya'/a}{zb'/b}.$$

This represents flow out along the major axis and in along the minor axis when a is increasing and b decreasing, and vice versa. When a' and b' both have the same sign, however, the secondary streamlines are those of a source or sink on the axis $y = z = 0$.

The next term in the pressure expansion, p_1 , is also independent of η and ζ , from (6.10) and (6.11), so that u_1 satisfies

$$(1/a^2)u_{1\eta\eta} + (1/b^2)u_{1\zeta\zeta} = -G_1(x) - [4(ab)'/a^3 b^3]Re(1 - \eta^2 - \zeta^2)^2,$$

where

$$G_1(x) = -dp_1/dx.$$

The solution of this that satisfies the boundary condition is

$$u_1 = Re(1 - \eta^2 - \zeta^2)(c_0 + c_1\eta^2 + c_2\eta^4 + c_3\zeta^2 + c_4\zeta^4 + c_5\eta^2\zeta^2), \quad (6.15)$$

where

$$\begin{aligned} c_0 &= G_1 a^2 b^2 / 2Re(a^2 + b^2) \\ &\quad + \alpha(33 + 608\delta^2 + 2238\delta^4 + 608\delta^6 + 33\delta^8), \\ c_1 &= -\alpha(66 + 850\delta^2 + 1074\delta^4 + 238\delta^6 + 12\delta^8), \\ c_2 &= -\alpha\beta(33 + 44\delta^2 + 3\delta^4), \\ c_3 &= -\alpha(12 + 238\delta^2 + 1074\delta^4 + 850\delta^6 + 66\delta^8), \\ c_4 &= -\alpha\beta(3 + 44\delta^2 + 33\delta^4), \\ c_5 &= 4\alpha\beta(3 + 34\delta^2 + 3\delta^4), \end{aligned}$$

and

$$\begin{aligned}\alpha &= 2b^2 A' / 45 A^3 \beta (1 + 15\delta^2 + 15\delta^4 + \delta^6), \\ \beta &= 1 + 6\delta^2 + \delta^4, \\ \delta &= b/a,\end{aligned}\tag{6.16}$$

$$A = ab.\tag{6.17}$$

G_1 is again determined from the volume flux condition, in the form

$$\iint u_1 \, d\eta \, d\zeta = 0$$

which unexpectedly simplifies to

$$G_1(x) = -2ReA'/A^3\tag{6.18}$$

and therefore depends on the area change, but not on the cross-sectional shape of the tube. This part of the solution has been expressed in terms of two new variables: δ , which is a measure of the eccentricity of the ellipse and always lies between 0 and 1, and A , the dimensionless cross-sectional area. In the application to elastic tubes it is found convenient to work with these quantities and a mean diameter, represented by

$$c = a + b.\tag{6.19}$$

The effect of inertia on the lubrication solution is expressed by the perturbations εu_1 and εG_1 to the velocity and pressure gradient. Each term is in fact proportional to εRe , which is the important small parameter. To see their effect, we look at the velocities and pressure drop in a tube whose elliptical cross-section varies in a given way. The cross-sectional area is taken to vary as

$$A = 1 - (729/32)x^4(1-x)^2$$

so that the minimum area of $\frac{1}{2}$ is achieved at $x = \frac{2}{3}$. The shape of the tube is fixed by specifying the relation between a and b , i.e. between c and δ . Two different relations are used, as follows:

(i) constant perimeter (as for rubber tubes) equal to 2π , so

$$\int_0^{\frac{1}{2}\pi} [1 - (1 - \delta^2) \sin^2 \theta]^{1/2} d\theta = \frac{\pi}{2a} = \frac{\pi(1 + \delta)}{2c}.\tag{6.20}$$

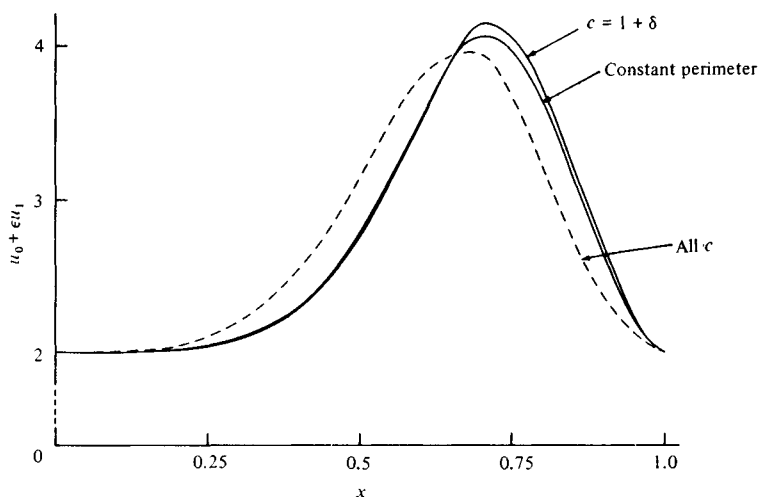


Fig. 6.8. The variation of velocity along the centre line of the rigid tube for the two relations between area and shape (represented by c). Broken curves, no inertia; continuous curves, $\epsilon Re = 1$. (After Wild *et al.*, 1977.)

- (ii) perimeter decreasing as area decreases; in view of the limited data, a simple model in which the length of the major axis remains constant as A decreases is chosen to give a qualitative indication of the behaviour of blood vessels. We thus choose

$$c = 1 + \delta = 1 + A.$$

Results are presented in three ways: the variation of u and p along the centre line of the tube (figs. 6.8 and 6.9) and the variation of u_1 across the semi-major and semi-minor axes (fig. 6.10). The constriction in each case accelerates the flow along the centre line (fig. 6.8), to a maximum velocity which is at $x = \frac{2}{3}$ when inertia is negligible ($\epsilon Re = 0$, broken curve), but which increases and occurs further downstream as inertia becomes more important (the continuous curves are for $\epsilon Re = 1$). The maximum pressure gradient also increases as inertia becomes more important (fig. 6.9), but occurs further upstream than in the absence of inertia, where $A' < 0$ in (6.18). It is interesting to note that the presence of inertia (mediated by the secondary motions) causes a deceleration of the flow in the centre of the tube as A decreases, but an acceleration at the edge of both the major and the minor axes (fig. 6.10). The

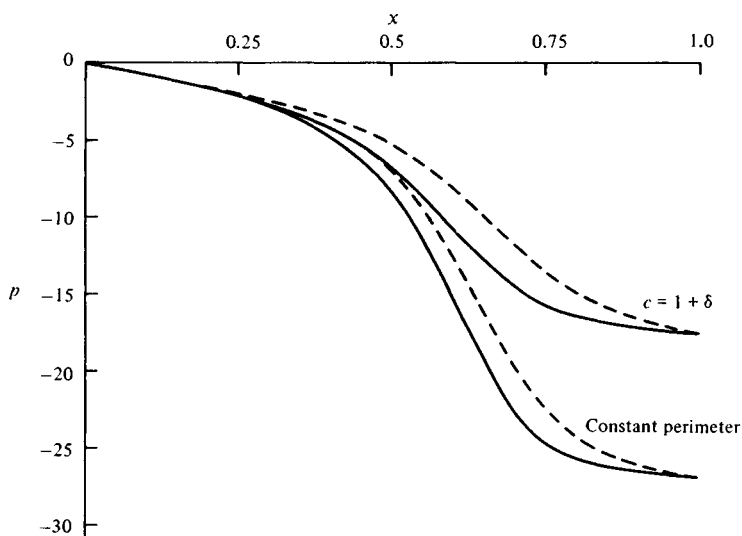


Fig. 6.9. The variation of pressure along the centre line of the rigid tube. (After Wild *et al.*, 1977.)

reverse is true as A increases again. This is in marked contrast with inviscid flow, where the secondary motions cause an acceleration near the wall on the major axis (as A increases), and a deceleration on the minor axis (Sobey, 1976*a*). In the case of constant major axis ($c = 1 + \delta$), the perimeter for a given area is smaller than in the other case. Thus the change in velocity and the pressure drop are also significantly smaller, because the cross-section is more nearly circular at each value of A . In this case $v_0 = 0$ (see (6.14)) and w_0 has the same sign as $b'\zeta$: the secondary streamlines are straight, and parallel to the minor axis.

6.2.2 Application to collapsible tubes

In this application the cross-sectional area of the tube at any value of x is assumed to depend only on the local transmural pressure, in the manner shown in fig. 1.10(*a*) and represented by the equation

$$\hat{p}_{tm} = \hat{P}_0 P(A), \quad (6.21a)$$

where \hat{P}_0 is a dimensional scaling factor, and P is a dimensionless function of A . As defined above, the area is made dimensionless by

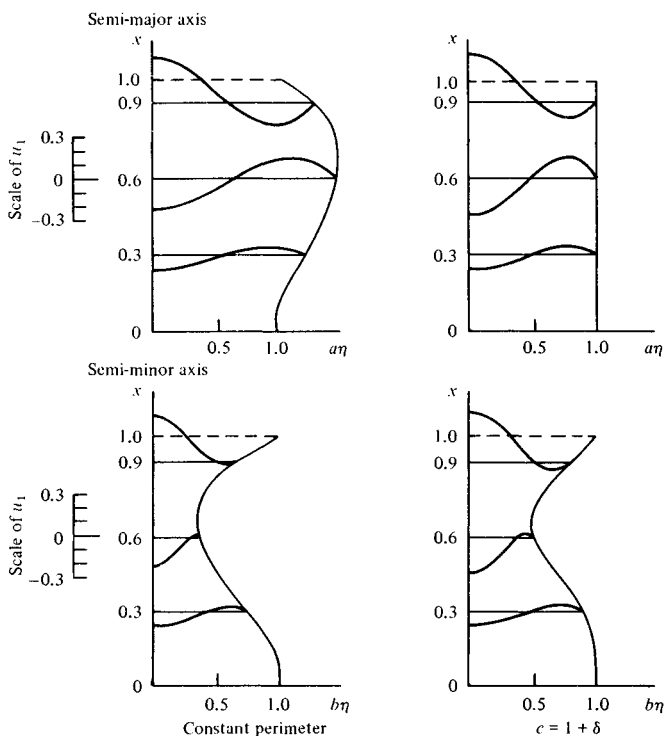


Fig. 6.10. First-order velocity profiles at three stations along the semi-major and semi-minor axes of the rigid tube. (After Wild *et al.*, 1977.)

dividing by πa_0^2 , and now we choose a_0 to be the radius of the tube at the transition between circular and elliptical cross-section (i.e. the tube is circular for $A \geq 1$, elliptical for $A < 1$). We then fix \hat{P}_0 as the value of \hat{p}_{tm} when the tube is just circular, i.e. by requiring that $P(1) = 1$. This elastic pressure-scale is different from the fluid dynamic pressure-scale used above (see (6.6)) so we introduce the dimensionless parameter

$$S = \epsilon Re \hat{p}_0 / \rho U_0^2 = \pi a_0^4 \hat{p}_0 / \mu L \hat{Q}, \quad (6.22)$$

where \hat{Q} is the flow-rate through the tube. Thus, for a given tube with given elastic properties, S can also be regarded as an inverse measure of flow-rate. If we stick to the convention that all pressures are non-dimensionalised with respect to $\rho U_0^2 / \epsilon Re$, then (6.21)

becomes

$$p_{tm} = SP(A). \quad (6.21b)$$

One of the experimental situations that we are attempting to model is that of a finite length of collapsible tube, with external pressure $(\rho U_0^2/\epsilon Re)p_c(x)$ given for all x , and with internal pressure given at the entrance, $x = 0$. Clearly then, the distribution of area with distance along the tube, and hence the relation between pressure drop and flow-rate down the tube, will depend on the transmural pressure at $x = 0$. Thus, another dimensionless parameter on which the flow will depend is

$$p_{tm}(0) = (\epsilon R/\rho U_0^2)[\hat{p}(0) - \hat{p}_c(0)];$$

this will determine the initial cross-sectional area, $A(0)$, from (6.21b). In computing the results, it is more convenient to specify $A(0)$, and derive $p_{tm}(0)$ from that equation.

For a given flow-rate and a given distribution of area, the pressure distribution inside the tube is determined from (6.12) and (6.18). For given distributions of external and internal pressure, the cross-sectional area is determined from (6.21b). Combining the two and using (6.19), we obtain the following ordinary differential equation for $A(x)$:

$$SP'(A) \frac{dA}{dx} = -\frac{dp_c}{dx} - \frac{4(c^2 - 2A)}{A^3} + \frac{2\epsilon Re}{A^3} \frac{dA}{dx}. \quad (6.23)$$

This is solved (by simple numerical integration) subject to the initial condition that $A(0)$ is given.

The elastic properties of the tube are represented by the function $P(A)$. This is specified to fit the experimental curve for veins given in fig. 1.10(a), in the form

$$P(A) = (1/A)[0.34(3A - 1) + 0.01(3A - 1)^5 + 0.1(3A - 1)e^{-5A/A^2}]. \quad (6.24)$$

Both curves are plotted in fig. 6.11. The first two terms within the square brackets are of the form specified by Rubinow & Keller (1972), and the last term is added to ensure that dA/dx remains finite as $A \rightarrow 0$ in (6.23), for otherwise negative areas are predicted and the model breaks down. Note that the area has reduced to

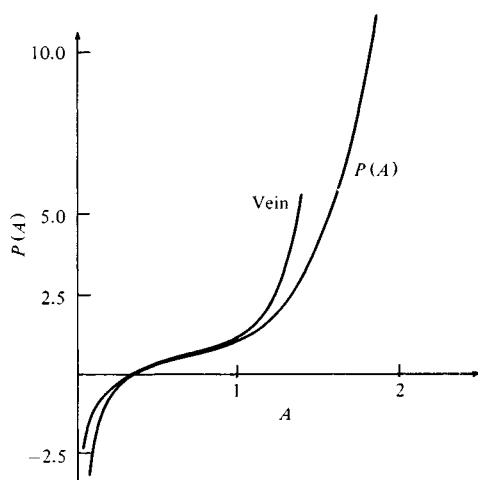


Fig. 6.11. Comparison of the function $P(A)$ with the transmural pressure–area relation for the canine vena cava (as shown in fig. 1.10(a)). (After Wild *et al.*, 1977.)

one-third of its reference value ($A = \frac{1}{3}$) when the transmural pressure is zero, which is appropriate for veins but not for rubber tubes. Note too that this pressure–area relation is more complicated, and probably less accurate, than that used in § 6.3 below, but it is retained so that Wild *et al.*'s results can be quoted directly. The qualitative behaviour of the results, at the present fairly low Reynolds numbers, will not be affected

The external pressure p_c could be taken to be constant. Instead we choose a form representative of a cuff inflated over part of the length, in the form

$$p_c(x) = ST\{1 - \exp[1 - 1/4(x - \frac{1}{2})^2]\}. \quad (6.25)$$

This is plotted in fig. 6.12; p_c is zero at the two ends of the collapsible segment ($x = 0$ and 1), and takes the maximum value ST at the mid-point, $x = \frac{1}{2}$. This corresponds to a dimensional cuff pressure of $\hat{T} = \rho U_0^2 ST / \epsilon Re = \hat{P}_0 T$ (see (6.22)). Thus, if the flow-rate is varied in a given tube with a given cuff pressure, T remains constant as S is varied.

The relation between the area and the shape of the cross-section must be specified, as in the last section. We shall present results only

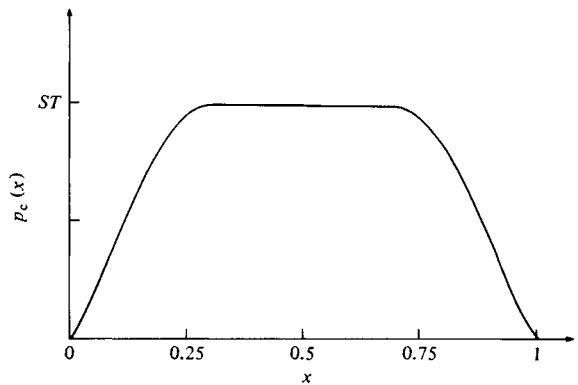


Fig. 6.12. The external pressure, $p_c(x)$, in the form of an inflated cuff. (After Wild *et al.*, 1977.)

for the case in which the major axis of the ellipse remains constant and the perimeter decreases during collapse (case (ii) above), i.e. in which

$$\begin{aligned} c &= 2A^{1/2} \quad \text{for } A \geq 1 \text{ (circular),} \\ c &= 1 + A \quad \text{for } A < 1 \text{ (elliptical).} \end{aligned} \tag{6.26}$$

Wild *et al.* (1977) also plotted results for the case $c = 2$, and they were qualitatively very similar.

Integration of (6.23) can proceed when the following parameters are specified: ϵRe , S , T , $A(0)$; the last of these determines $p_{tm}(0)$ from (6.21*b*), and this is the same as $p(0)$ because $p_c(0) = 0$. Table 6.1 gives the radii, lengths, mean velocities, Reynolds numbers and

Table 6.1. *Values of parameters in veins*

| Vein | \hat{A} (cm ²) | \hat{L} (cm) | U_0 (cm s ⁻¹) | Re | ϵRe |
|--------------------|------------------------------|----------------|-----------------------------|-----------|---------------|
| Inferior vena cava | 0.5 | 30 | 15–40 | 400–1000 | 7–17 |
| Medium-sized vein | 0.2 | 2 | 1–10 | 10–100 | 1–10 |
| Venule | 0.002 | 0.15 | 0.2–0.5 | 0.02–0.05 | 0.0003–0.0007 |

values of εRe (where ε is taken to be the radius-length ratio of the whole vein) for three typical canine veins of different sizes. We can see that the present theory is likely to be inapplicable to large veins, but applicable to medium-sized and small veins where εRe remains below 2. The pressure-area relation given by (6.24) (and fig. 6.11) was derived for large veins, and is therefore unlikely to be completely accurate when applied to small veins, even when scaled with a different value of A_0 , but no further information is available. According to fig. 6.11, \hat{P}_0 takes a value close to 1.0 kN m^{-2} , and we therefore choose this to be its value. The numbers given in table 6.1 then show that the parameter S (see (6.22)) can vary over a very wide range, from about 30 to about 10^4 . The results presented below do not cover such a wide range, because they prove to be fairly insensitive to S when S is large, since the hydrodynamic pressure drop is then small compared with that required to make a significant change in tube area. T is taken to vary between 0 and 5, at which value the maximum cuff pressure is $5\hat{P}_0$. The initial area $A(0)$ is taken to be greater than, equal to, and less than the area ($A = 1$) at which the cross-section begins to become elliptical.

In fig. 6.13 we plot the cross-sectional area A as a function of distance x along the tube for various values of the flow-rate parameter S . The continuous curves are with inertia ($\varepsilon Re = 1$) and the broken curves without ($\varepsilon Re = 0$). The external pressure is constant ($T = 0.5$) and the initial area is constant ($A(0) = 1.1$). The main feature of the results is that there is a critical flow-rate (proportional to S^{-1}) above which the area becomes very small just downstream of the peak external pressure, and does not recover further downstream where the external pressure returns to zero. The critical value of S , say S_0 , is about 30 from fig. 6.13. The results are clearly very sensitive to the presence of inertia near this critical flow-rate, and predictions that ignore it are likely to be in error. The present predictions are also inaccurate for εRe as large as 1, when $S \approx S_0$, as can be seen from the large difference between the zero-inertia and the non-zero-inertia curves, but they indicate the qualitative effect of inertia. Error is also introduced by the rapid rate of change of A with x , which indicates that the effective value of ε may not be very small.

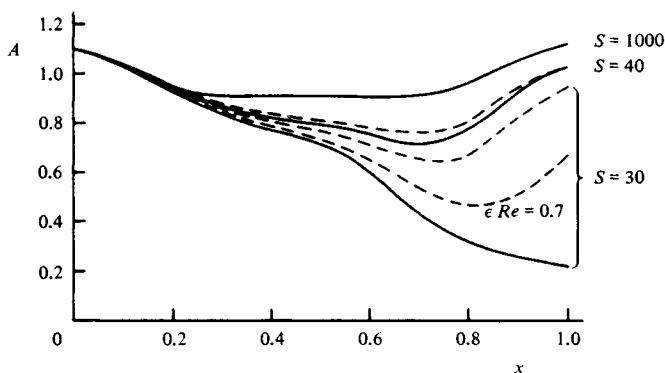


Fig. 6.13. Cross-sectional area, A , of the elastic tube as a function of x for various values of the flow-rate parameter, S . $c = 2\sqrt{A}$ for $A > 1$, $c = 1 + A$ for $A \leq 1$. Broken curves, zeroth-order solution ($\epsilon Re = 0$); continuous curves, with first-order inertial correction ($\epsilon Re = 1$). (After Wild *et al.*, 1977.)

It is clear that the pressure drop required for a given flow-rate (i.e. the resistance) will be significantly greater for $S < S_0$ than for $S > S_0$. This is confirmed by fig. 6.14, in which the pressure is plotted against x for the same case as shown in fig. 6.13.

In fig. 6.15, the area at the downstream end of the tube, $A(1)$, is plotted against the external pressure, T , again for various values of S and for $\epsilon Re = 0, 1$. This indicates how the critical value S_0 increases with T , so that smaller and smaller flow-rates are required to generate collapse as T increases. Once more we see that the effect of inertia is small except when S is close to S_0 .

In order to make some comparison with the experiments described in § 6.1, we wish to plot the dimensional pressure drop, $\hat{p}_1 - \hat{p}_2$, as a function of flow-rate, \hat{Q} , for given values of external pressure, \hat{p}_c , and for given conditions upstream and down. In dimensionless terms, this requires that we plot $(p_1 - p_2)/S = (\hat{p}_1 - \hat{p}_2)/\hat{P}_0$ against S^{-1} for fixed T . In fig. 6.16 we present such plots for various values of T , in conditions where the upstream area $A(0)$, and hence the upstream pressure $\hat{p}(0)$, are held constant; for these curves $A(0) = 1.1$ and we have considered only the case of constant major axis. These curves are clearly the same shape as

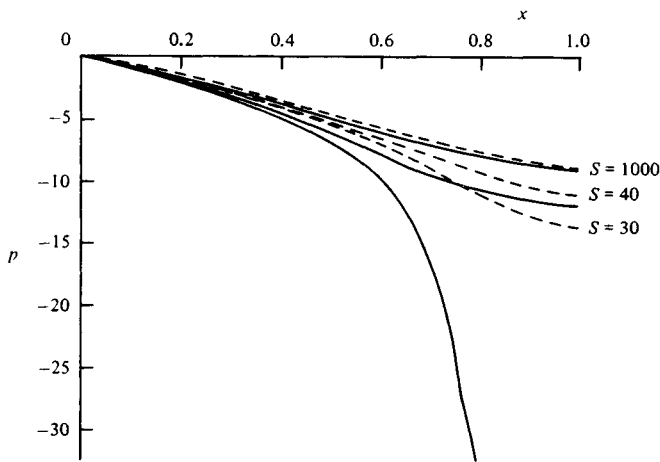


Fig. 6.14. The variation of pressure along the centre line of the elastic tube for various values of S . $c = 2\sqrt{A}$ for $A > 1$, $c = 1 + A$ for $A \leq 1$. Broken curves $\varepsilon Re = 0$; continuous curves, $\varepsilon Re = 1$. (After Wild *et al.*, 1977.)

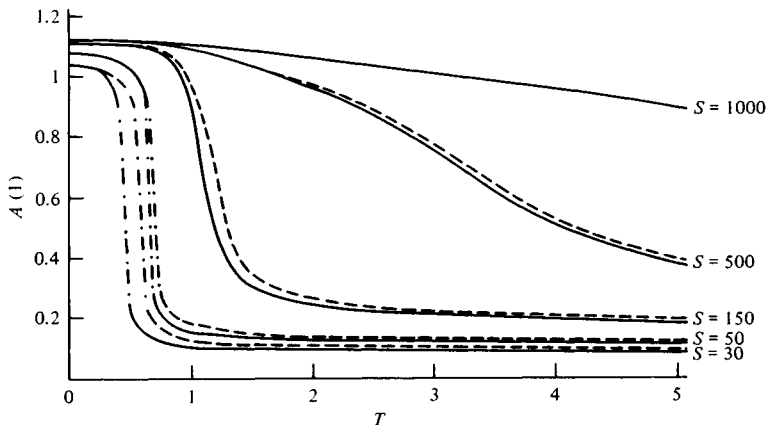


Fig. 6.15. Cross-sectional area at the downstream end of the tube, $A(1)$, as a function of the external pressure, T , for various values of S . $c = 2\sqrt{A}$ for $A > 1$, $c = 1 + A$ for $A \leq 1$. Broken curves, $\varepsilon R = 0$; continuous curves, $\varepsilon R = 1$; dot-dash parts of curves, points that have not been computed. (After Wild *et al.*, 1977.)

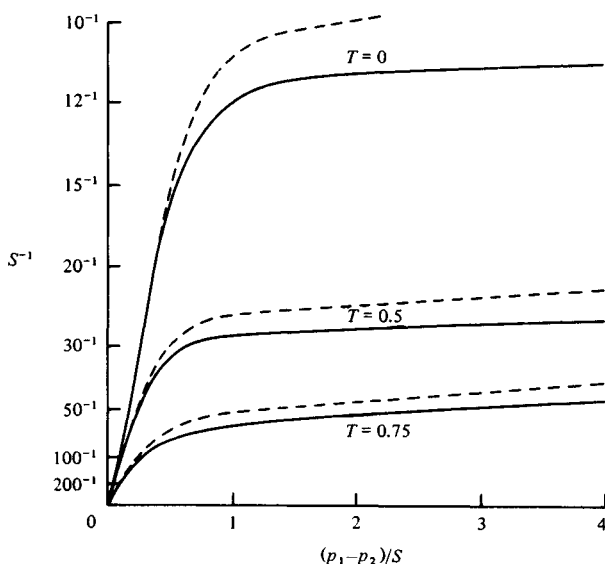


Fig. 6.16. Pressure drop along the tube as a function of the flow-rate, S^{-1} , for constant upstream area and pressure. The curves are plotted for three different values of external pressure, and for $\varepsilon Re = 0$ (broken curves) and $\varepsilon Re = 0.5$ (continuous curves). (After Wild *et al.*, 1977.)

those shown in figs. 6.1(b) and 6.5(b) and clearly demonstrate that an increase in driving pressure above a critical value does not increase the flow-rate. In order to make quantitative comparison with experiment, we must estimate the values of the dimensionless constants for Brecher's (1952) experiments on both the canine vena cava and rubber tubes. All the necessary data are not given by him, but we can take the radius of the vena cava to be about 0.5 cm (tables 1.1 and 6.1), and suppose a reasonable value of ε to be 0.1 (the axial length-scale is thus taken to be 5 cm, shorter than the vessel length, but possibly an overestimate for a typical length-scale during collapse). A flow-rate, \dot{Q} , of $4 \text{ cm}^3 \text{ s}^{-1}$ (fig. 6.1(b)) means an average velocity of 5 cm s^{-1} , so when $\nu = 4 \times 10^{-6} \text{ m}^2 \text{ s}^{-1}$ as for blood, the Reynolds number $Re \approx 62$ and $\varepsilon Re \approx 6.2$. Furthermore, if we take $\hat{P}_0 = 1 \text{ kN m}^{-2}$, as for the vena cava in the experiments of Moreno *et al.* (1970) (fig. 1.10(a)), the parameter S is seen to be about 2500. The pressure drops in fig. 6.1(b) of 0–50 cmH₂O, i.e. of 0–5 kN m⁻², are equivalent to values of $(p_1 - p_2)/S$ of 0–5. Thus the

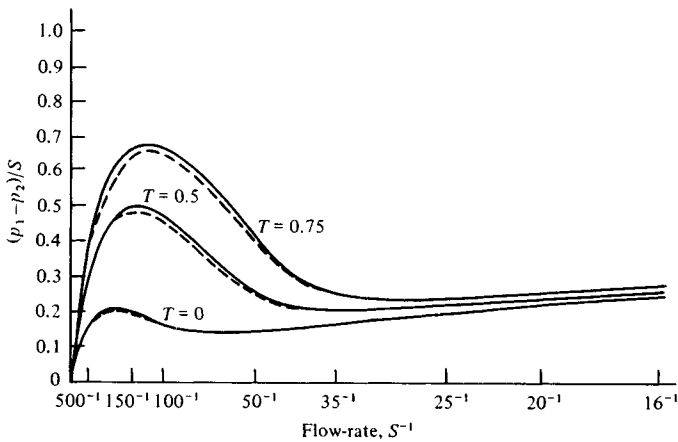


Fig. 6.17. Pressure drop along the tube as a function of the flow-rate, S^{-1} , for constant downstream resistance. The curves are plotted for three different values of external pressure and for $\epsilon Re = 0$ (broken curves) and $\epsilon Re = 0.5$ (continuous curves). (After Wild *et al.*, 1977.)

curve of fig. 6.1(b) has similar abscissa to that of fig. 6.16, but is squashed down to very small values of the ordinate; in the experiments the external pressure was presumably associated with respiration, and T would have been in the neighbourhood of 0.75. A similar conclusion is reached in the case of Brecher's rubber-tube experiments (fig. 6.5(b)), since he used tubes comparable in size with the vena cava. The value of \hat{P}_0 was presumably smaller in this case (cf. $\hat{P}_0 \approx 0.2 \text{ kN m}^{-2}$ from fig. 1.10(a) or $\hat{P}_0 \approx 0.5 \text{ kN m}^{-2}$ from fig. 1 of Katz *et al.* (1969)) but the flow-rates were larger ($6 \text{ cm}^3 \text{ s}^{-1}$) and S will therefore have been nearly as large as in the vena cava.

The discrepancy in scale between the theoretical and experimental curves must be principally a consequence of the fact that the theory has been developed for $\epsilon Re \ll 1$, while in the experiments $\epsilon Re \approx 6$. Thus the viscous pressure drop in the experiments must have been much less than the dynamic pressure changes experienced by the flow as it passed through the constriction, and the theory cannot be relevant. The fact that the curves have qualitatively the same shape is a consequence of the fact that the constriction causes enhanced pressure drop at high Reynolds number as well as at low Reynolds number. The mechanism is of

course different, probably being associated with separation of the flow from the constriction, rather than enhanced viscous stresses (see § 6.3). If the dynamic pressure drop were used instead of the viscous in the non-dimensionalisation, the corresponding values of S would be reduced by a factor εRe , which reduces the 2500 estimated above to about 400, and therefore puts the experiments and theory on a similar scale.

In fig. 6.17 we plot the same quantities as in fig. 6.16, but for a different experiment. This time we keep the downstream resistance \hat{R}_2 constant, as in the experiments of Conrad (1969), which led to figs. 6.3 and 6.4. Constant \hat{R}_2 means a constant ratio between \hat{p}_2 and \hat{Q} , or (in dimensionless terms) a constant value of $p_2 = \varepsilon \pi a_0^3 \hat{p}_2 / \hat{Q}$. This means that the one-point boundary condition to be applied to (6.23) is that $A(1)$ is given by

$$P[A(1)] = p_2/S.$$

The higher the flow-rate, the higher is S^{-1} and the higher is $A(1)$, so that collapse is less; integration of (6.23) will determine $A(0)$ and hence p_1 . In fig. 6.17, the constant value of p_2 is taken to be 50, which when $\varepsilon = 0.07$ and $a_0 = 0.63$ cm corresponds to a downstream resistance of $91 \text{ N m}^{-2} \text{ per cm}^3 \text{ s}^{-1}$, i.e. of 6.9 mmHg per $10 \text{ cm}^3 \text{ s}^{-1}$, which is comparable with the smallest of the downstream resistances used by Conrad (see fig. 6.3(b)). The 'inertial' curves of fig. 6.17 are for $\varepsilon Re = 0.5$. The main features of this figure are the facts that $\Delta \hat{p}$ is a multiple-valued function of \hat{Q} , as in the experiments, and that this phenomenon is independent of the presence of inertia. As in the case of fig. 6.16, however, the quantitative comparison is poor, because of the large value of S appropriate to the experiments: in Conrad's system ($a_0 = 0.63$ cm, $\hat{P}_0 \approx 0.5 \text{ kN m}^{-2}$, $\varepsilon = 0.07$), a flow-rate of $2.5 \text{ cm}^3 \text{ s}^{-1}$ (see fig. 6.3(c)) corresponds to $S \approx 10^4$. Once more the discrepancy can be attributed to the dominance of the dynamic pressure drop over the viscous pressure drop in Conrad's high-Reynolds-number experiments ($\varepsilon Re \approx 8.1$).

When self-excited oscillations occur in collapsible tubes, they do so on the descending section of the curve of pressure drop against flow-rate, as shown in fig. 6.3(c). It is on the corresponding section of the curves in fig. 6.17 that attention is currently being focussed in

an analysis of unsteady flow whose aim is to predict a critical value of εRe above which oscillations can occur. The basic lubrication theory in the unsteady case is the same as in the steady case, but calculation of the effects of inertia (which must be included for oscillations to be possible) presents a major problem. The problem is that in order to calculate the first-order secondary velocities (such as those in (6.14) for the steady case) it is necessary to know the velocity components on the elliptical boundary, which varies slowly in both time and space. Calculation of the normal velocity component is straightforward, but that of the tangential component requires a more detailed knowledge of the elastic properties of the tube wall than we have previously assumed. One possibility is to assume that the length of every element of the cross-section's perimeter varies in direct proportion to the total perimeter (and would therefore remain virtually constant in the case of a rubber tube); thus the paths of each element could be calculated and their velocities deduced. Another possibility would be to assume linear elasticity, and treat the wall as a membrane in which the local tension is everywhere proportional to the radius of curvature (since the internal pressure is uniform across the cross-section in both the zeroth- and the first-order approximations). However, both approaches lead to a considerable increase in complexity and we have restricted ourselves initially to tubes whose cross-section remains circular (as in the steady theory of Manton (1971)) but that still have pressure–area relations of the form of fig. 6.11. The fluid mechanics is now simple, but leads to partial differential equations for $p_0(x, t)$, $p_1(x, t)$ and $A(x, t)$, instead of the ordinary differential equation (6.23), and these have not yet been solved.

6.3 A lumped-parameter model for self-excited oscillations

6.3.1 *Physical mechanisms*

As will become clear in the rest of this chapter, there are several different mechanisms that could each drive the self-excited oscillations observed in the model experiments. In proposing a theory for the phenomenon, therefore, it is not enough to demonstrate that one particular mechanism *can* cause oscillations in some experiments; it is necessary, instead, to consider one particular

experiment and to construct a theory for it, firmly based on sound physical principles, which will show to what extent the several mechanisms contribute to the oscillations in that case. The models to be described in this section and the next have not yet reached that stage, but it will be seen that there are at least four possible mechanisms by which steady flow can become unstable, and the quantitative details suggest that any one of them may be relevant to the observed oscillations of Conrad (1969). Any particular experiment, therefore, should be analysed in terms of all of these mechanisms, not just one. The exposition of the models reveals gaps in the 'sound physical principles' on which all such models must be based, demonstrating that a complete theory is still some way off, because the gaps must be filled, either by theory or by experiment.

The models concern the experiment depicted in fig. 6.2, and described on pp. 304–7, in which a length of collapsible tube is supported between two rigid tubes, each having constant resistance. Suppose that initially the flow is steady and the chamber pressure is zero or negative, so that the collapsible segment is distended and has an approximately constant, circular cross-section. We assume that this configuration is stable to small disturbances. Now let us consider what happens if at time $t = 0$ the chamber pressure is suddenly raised to a new constant value, \hat{p}_c .

If \hat{p}_c is sufficiently small, then the transmural pressure \hat{p}_{tm} will everywhere remain greater than the critical value below which collapse begins. As can be seen from fig. 1.10(a), that value is close to zero for rubber tubes, though not for veins; detailed calculations of the critical value were made by Anliker & Raman (1966) in their analysis of the initiation of buckling in a fluid-filled cylindrical shell of linearly elastic material.

If \hat{p}_c is large enough, however, \hat{p}_{tm} will exceed the critical value and the tube will begin to collapse at its downstream end. Since the Reynolds number is large, the time-scale for the collapse will be much shorter than the viscous diffusion time, and the perturbation to the initial flow will be effectively inviscid. Therefore the flow will be accelerated through the narrowed segment, and the fluid pressure will fall in the manner described by Bernoulli's equation (even when the unsteady, reactive pressure is taken into account). Note that the reactive pressures generated in the fluid by the collapse

process will be propagated both upstream and downstream by a pressure wave in the tube wall, whose speed can be calculated from the theory of chapter 2. When the collapsible segment is short, and the upstream tube effectively rigid, the propagation will be virtually instantaneous. The pressure fall at the constriction will accentuate the collapse, which will continue until *either* a new, stable equilibrium is reached (because the tube is very stiff when almost completely collapsed) *or* some other effect comes into play. In fact, various 'other effects' must come into play whether or not there is a theoretical stable equilibrium.

The first such effect is the development of significant energy losses as the collapse proceeds. The inviscid disturbance to flow in the core will cause viscous boundary layers to develop on the walls, which can initially, no doubt, be analysed by the theory of Smith (1976*d*) and Duck (1979). When the cross-sectional area of the constriction becomes very small, and hence the velocity of the flow through it becomes large, the boundary layers will fill the cross-section and the viscous energy dissipation in this narrow region of high shear will become important. In a quasi-steady, quasi-parallel flow model this could be represented by the high resistance of a narrow tube, as described by (6.13). Probably more important, however, is the fact that unless the wall slope is kept extremely small (e.g. by a large longitudinal wall tension) the flow will separate at approximately the narrowest point, and an asymmetric jet will emerge into the downstream rigid tube. There may also be upstream separation (Smith, 1977*b*), but since the experiments generally indicate that the narrowing of the tube upstream of the narrowest point is much more gradual than the subsequent widening (fig. 6.18), this is not inevitable, and in any case the head loss associated with it will not be as dramatic as with the downstream separation. The downstream jet will also normally become turbulent unless the Reynolds number at the constriction is below about 500 (cf. p. 314). Now the processes of flow separation and jet instability each take a short but finite time, related to the convection time-scale \hat{a}_0/\hat{U} , where \hat{a}_0 is the undisturbed tube radius and \hat{U} the velocity through the constriction. On such a time-scale, therefore, we expect significant energy losses to develop, in addition to the direct viscous losses already discussed. These losses will cause a

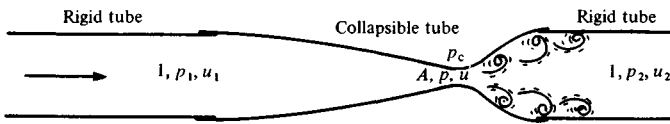


Fig. 6.18. Sketch of collapsible segment specifying the areas, pressures and velocities at three stations, as required by the lumped-parameter model.

sharp pressure drop downstream of the constriction and a dramatic reduction in the flow-rate. This will in turn generate a rise in pressure at, and upstream of, the constriction, and this pressure rise will first slow down the collapse, then reverse it. There will normally be an equilibrium state in which there is significant energy loss and some degree of collapse (see § 6.3.3) below. If this equilibrium is stable, the system will tend to it (unless there is sufficient inertia in the motion of the wall and the fluid for the area to return to its open position, and possibly beyond, in which case the separation bubble would be swept away and the cycle would be free to start again). If the equilibrium is unstable, on the other hand, the system will either tend to another equilibrium that exists at the same values of the parameters, or oscillations will occur because the tube is so stiff at both very large and very small areas that the area cannot either increase or decrease indefinitely.

Circumstantial support for the importance of flow separation in the self-excited oscillations observed by Ur & Gordon (1970) comes from their detailed discussion. They report the following sequence of events in an oscillation whose period is approximately 70 ms, based on the recordings of fig. 6.7 corrected for the time taken by pressure waves to propagate to the measuring sites (the collapsible segment was 25 diameters long). About 3 ms before maximal closure of the constriction, there began a large (200 mmHg) and rapid drop in downstream pressure, lasting about 5 ms; this may be interpreted as the development of separation. Ur & Gordon associate it with deceleration of the column of fluid downstream of the constriction, which is, of course, an inevitable correlate of the pressure fall. As the tube closes there is also a sharp, but less large (55 mmHg), rise in upstream pressure, lasting about 2 ms, which is presumably the reactive pressure rise also mentioned above. Following maximal closure of the tube, the downstream

pressure returns, within 8 ms, to a level of 20–25 mmHg, and the upstream pressure falls to about 35 mmHg in 22 ms. These are elevated above the undisturbed state because of the distension of the upstream segment. Such relatively gradual pressure changes are associated with the re-opening of the tube, which is maximally open (having overshoot its undisturbed configuration) after 32 ms. In the next 36 ms there is a gradual reduction in tube area, before sudden collapse again takes place and the cycle restarts.

Implicit in the above discussion is the assumption that the elastic behaviour of the tube at each cross-section can be described by the same pressure–area curve, such as that in fig. 1.10(*a*). It has been pointed out by J. M. Fitz-Gerald (personal communication) that this is unlikely to be true if the tube is either thin-walled or quite long, when the segment of flexible tube upstream of the constriction may play an important role. As the flow at the constriction is slowed down by the energy losses caused by separation, there will tend to be more flow into the upstream segment than out of it, so that it will become distended. This distension will then tend to pull open the constricted segment through longitudinal tensile forces. If the longitudinal tension in the undisturbed wall is sufficiently great, and if the wall is sufficiently thin, then the restoring force associated with this tension could dominate that associated with the resistance to transverse bending as the cross-section changes shape (cf. § 1.1.4); a numerical model incorporating this possibility has recently been developed by Collins & Tedgui (1979). The model to be presented later in this section will ignore longitudinal tension, and is therefore likely to be relevant only to relatively short, relatively thick-walled tubes. Future developments require the incorporation of longitudinal tension and longitudinal curvature into the model on the lines proposed by Collins & Tedgui (1979), by Griffiths (1975*c*) and by J. M. Fitz-Gerald. However, it is unlikely to affect the basic fluid mechanics that underlie the oscillations predicted by the lumped-parameter model outlined below.

What lumped-parameter models inevitably do ignore are phenomena directly associated with the continuous variation of cross-sectional area and velocity in the real system. Thus if the flow in the longitudinally slowly varying segment upstream of a steady constriction is intrinsically unstable to a local mechanism, then the

steady state will be unstable even if the lumped-parameter model predicts stability. This is shown to be a real possibility by the analysis of § 6.4, where an instability mechanism analogous to that of roll-waves in open channel flow (Dressler, 1949) is shown to operate in elastic tubes.

Another potentially important effect, associated with the continuously varying system, has also been ignored hitherto. It comes from the fact that an elastic tube can support pressure waves, as described in chapter 2. 'Choking' is therefore predicted to occur if the local fluid speed anywhere becomes equal to the local speed of propagation of such waves. This effect is also investigated briefly in § 6.4, and may well be relevant in many experiments in which oscillations have been observed.

6.3.2 *Mathematical formulation*

The detailed, non-linear, three-dimensional, unsteady fluid mechanics of the collapse process is dauntingly complex, and in order to formulate a tractable model some drastic simplifications have to be made. Here we reduce the whole system to a third-order set of ordinary differential equations with the consequence, as already indicated, that many real phenomena cannot be described. Several interesting phenomena are described, however, and it is hoped that, if the model is carefully derived, they may correspond to some of those observed experimentally. The model is similar in many respects to that proposed by Katz *et al.* (1969), but there are important differences, so that although the present system is of lower order, it is somewhat more soundly based. Moreover, the very fact of its being of lower order means that greater analytical (and hence physical) understanding can be obtained; in view of the variety of behaviour that is predicted for different values of the parameters, this is essential. Another similar model has been proposed by Schoendorfer & Shapiro (1977), who analysed a collapsible tube device that might act as a vocal source for laryngectomised patients. The oscillations of the collapsible tube walls would replace those of the vocal chords as the basis for speech.

The most drastic assumption is to assert that the geometrical configuration of the collapsible segment can be completely specified by a single variable, the cross-sectional area, \hat{A} , at the narrowest

part of the constriction, close to the downstream end (fig. 6.18). We also assert that the tube-wall elasticity can be fully taken into account by specifying a single-valued functional relation between the transmural pressure, \hat{p}_{tm} , and \hat{A} . So we beg all the elastic questions not only by choosing a given function relating \hat{p}_{tm} and \hat{A} at each value of \hat{x} , the axial distance, but also by saying that the narrowest portion of the tube is representative of the whole segment. This is equivalent to the statement that the configuration of the tube, the longitudinal shape as well as the transverse shape, is completely specified when \hat{A} is specified; no independent distension of the upstream segment relative to the constriction is possible. Thus the presence or absence of longitudinal tension and/or curvature in the wall is not important, except in its effect on the pressure–area relation. The main advantage of the assumption, of course, is that the final differential equation for \hat{A} is ordinary (in \hat{t}) not partial (in \hat{t} and \hat{x}), and can be solved relatively simply.

In the equations to be presented, the area \hat{A} is made dimensionless with respect to the upstream and downstream area \hat{A}_0 , and all velocities are non-dimensionalised with respect to an arbitrary scale, \hat{U}_0 . Pressures and time are scaled with respect to $\rho \hat{U}_0^2$ and to \hat{a}_0 / \hat{U}_0 respectively, where \hat{a}_0 is the radius of the rigid tubes and ρ is the fluid density. The collapsible segment is depicted in fig. 6.18 with the dimensionless area, pressures and velocities marked at the three stations to be considered: upstream (suffix 1), downstream (suffix 2) and at the constriction (no suffix). The dimensionless external pressure is p_c . The straight lines represent the rigid tubes, upstream and downstream. The only independent variable is the dimensionless time, t ; the equations governing this model can be written down as follows.

Elasticity. As already discussed, the elastic properties of the collapsible segment are represented by a single equation relating the transmural pressure at the narrowest point to the cross-sectional area there:

$$p - p_c = P(A). \quad (6.27)$$

If quantitative agreement with experiment is hoped for, the function $P(A)$ should be measured independently for every piece of

collapsible tube used; graphs like those of fig. 1.10(a) would be obtained. Here, however, we shall use a simple functional form to represent rubber tubes (in the same way that (6.24) was used to represent veins). We shall incorporate into it the similarity solution derived by Flaherty *et al.* (1972*a*) for the relation at small values of A when there is no longitudinal variation. This is based on the fact that when the opposite walls of the tube are in line contact (fig. 6.19(a)) the original radius of the tube cannot be relevant to the pressure–area relation. The only length-scale available is a typical radius of curvature, say R . Now the analysis of bending of the tube wall (§ 1.1.4) shows that

$$1/R = M/EI, \quad (6.28)$$

where M is the bending moment (per unit length of the tube), I is the moment of inertia of the wall cross-section (per unit length) and E is the Young's modulus of the material, assumed constant. Of these quantities only M depends on R , and is proportional to the bending force (per unit length) times a distance, i.e. to $\hat{p}_{tm}R$ times R . Thus (6.28) shows that the transmural pressure, \hat{p}_{tm} , is proportional to R^{-3} , which is proportional to $\hat{A}^{-3/2}$. We follow Shapiro (1977) and use the simplest form for $P(A)$ that is consistent with this result as $A \rightarrow 0$ and that represents a change to circular cross-section (and greater stiffness) at zero transmural pressure (cf. fig. 1.10(a)); this is

$$\left. \begin{aligned} P(A) &= P_0[1 - (A_c/A)^{3/2}], & A < A_c, \\ &= 10P_0(A/A_c - 1), & A > A_c, \end{aligned} \right\} \quad (6.29)$$

and is plotted in fig. 6.19(b). Here A_c is the (dimensionless) area at which the transition takes place; in an experiment one might expect A_c to be slightly less than 1, on the assumption that a little distension is required to fit the flexible tube over the rigid ones, but in all subsequent calculations we shall take $A_c = 1$. This cannot have great qualitative significance. P_0 is equal to a dimensional pressure-scale, \hat{P}_0 , divided by $\rho\hat{U}_0^2$; its value will be chosen later. The factor 10 in the second of equations (6.29) is a rather arbitrary representation of the greater stiffness of the circular cross-section.

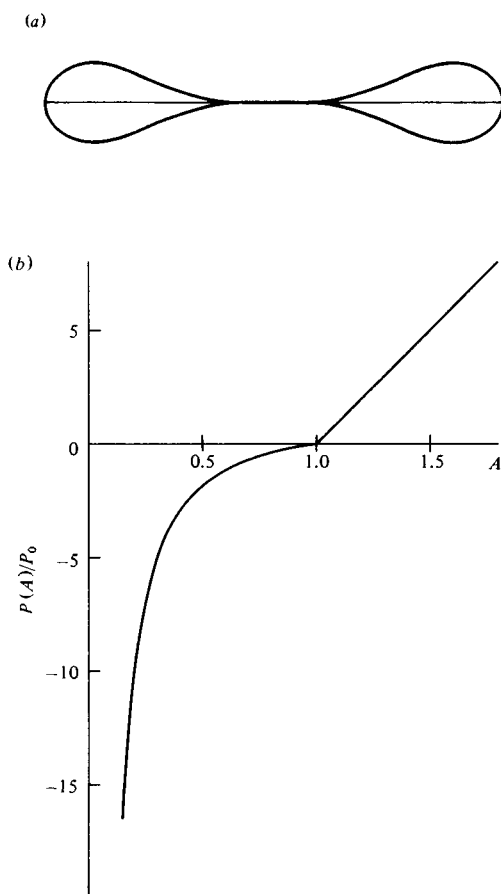


Fig. 6.19. (a) Shape of tube cross-section when there is line contact between opposite sides and a similarity solution for $P(A)$ exists. (After Flaherty *et al.*, 1972*a*.) (b) Graph of the pressure–area relation (6.29).

In some experiments it may be important to include the inertial and viscoelastic properties of the tube wall. In that case, the extra terms

$$\eta \dot{A} + I_w \ddot{A}$$

should be added to the right-hand side of (6.27), where η and I_w are constants representing wall viscosity and inertia respectively, and an overdot means d/dt . These terms do not increase the order of the

system, but merely add to the number of imprecisely known constants in the model; they are therefore set to zero in all present calculations.

Conservation of mass. Equations are required to relate the difference between the inflow and outflow at the ends of the collapsible segment to the rate of change of its volume. Recognising that in most experiments the collapse occurs close to the downstream end of the flexible segment, we suppose that all volume change occurs upstream of the narrowest point. Thus the flow-rate through the constriction is equal to the flow-rate downstream,

$$uA = u_2, \quad (6.30)$$

while, for the upstream segment

$$u_1 - uA = l\dot{A}_v, \quad (6.31)$$

where l is the dimensionless length of the upstream segment and A_v is its average area. In the absence of detailed experimental data, we take

$$A_v = \frac{1}{2}(1 + A), \quad (6.32)$$

but it must be emphasised that this is somewhat arbitrary. Note too that there would be no difficulty in including some downstream compliance in (6.30), with a much smaller value of l , for example, but in the interests of simplicity we omit it.

Momentum equations in the rigid tubes. The upstream and downstream rigid tubes may be long, straight tubes, along which the pressure drop is proportional to the flow-rate, or they may incorporate variable constrictions (cf. Conrad, 1969) which would mean that at all but the smallest flow-rates the pressure drop would be proportional to the square of the flow-rate. They will probably be a combination of the two, and we choose to represent them by resistances, \hat{R}_1 and \hat{R}_2 , that are non-decreasing functions of the magnitudes of the velocities, \hat{u}_1 and \hat{u}_2 , through them. In most of the numerical calculations, however, \hat{R}_1 and \hat{R}_2 are taken to be constants. The fluid in the rigid tubes will also have inertia, and we choose to represent this linearly from the start. If we suppose that the flow enters the upstream rigid tube from a reservoir of constant

dimensionless head, P_1 , and that it leaves the downstream rigid tube into atmosphere at zero pressure, the momentum equations for these two tubes are

$$P_1 - p_1 = R_1 u_1 + I_1 \dot{u}_1, \quad (6.33)$$

$$p_2 = R_2 u_2 + I_2 \dot{u}_2, \quad (6.34)$$

where $R_{1,2} = \hat{R}_{1,2}/\rho \hat{U}_0$ and $I_{1,2}$ are corresponding dimensionless inertances.

Momentum/energy equation downstream of the constriction. We have already emphasised the importance of the unsteady head loss associated with the development of a separated, probably turbulent, jet downstream of the constriction as its area decreases, and its subsequent disappearance as the tube opens up again. Since some of the observed oscillations had periods as low as 0.02 s (Ur & Gordon, 1970), comparable with a typical convection time \hat{a}_0/\hat{U}_0 , the phase relation between the unsteady head loss and (say) the velocity \hat{u} at the constriction is likely to be important. The use of a quasi-steady relation is unlikely to be truly representative. However, this is one of the areas of fluid mechanics about which almost nothing is yet known[†] (except for some limited results on sinusoidally oscillating flow through a fixed constriction by Young & Tsai (1973*b*)), and we have no alternative but to use the quasi-steady relation here.

For steady separated flow through a sharp constriction, the integral form of the momentum equation can be applied to the fluid between the constriction and a downstream station at which the mean velocity profile is approximately flat (where the jet has spread to the side-walls: fig. 6.20). When the jet is turbulent, this is not far downstream. Use of the equation requires a knowledge of the pressure on the downstream facing walls of the constriction; this must be approximately uniform and equal to the pressure at the constriction, for otherwise the lateral pressure gradient would not permit an approximately parallel-sided jet to form. The momentum

[†] Dr T. W. Secomb and Dr C. D. Bertram at the University of Cambridge are currently working to fill this gap, both theoretically and experimentally.

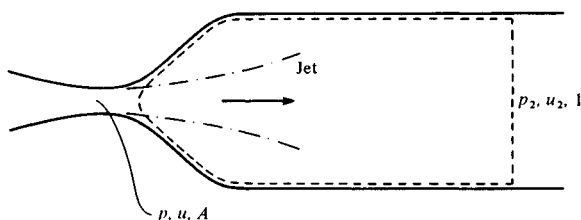


Fig. 6.20. Control surface for use with the integral momentum equation, leading to (6.35).

equation then gives

$$p + Au^2 = p_2 + u_2^2,$$

on the assumption that the longitudinal viscous shear force on the tube walls makes a negligible contribution. Together with (6.30) this gives

$$p - p_2 = -f(A)u_2^2, \quad (6.35)$$

where

$$f(A) = 1/A - 1, \quad \text{if } A < 1, u_2 > 0. \quad (6.36a)$$

Young & Tsai (1973*a*) made some measurements on steady flow through symmetric and asymmetric smooth constrictions of two different areas, and fitted their results to the equation

$$p_1 - p_2 = K_1 u_2 + \frac{1}{2} K_2 u_2^2 (1/A - 1)^2,$$

which is equivalent to the above if there is no head loss upstream of the constriction, if $K_1 = 0$ and if $K_2 = 1$. Young & Tsai's results indicated different values of K_2 , which, however, always lay in the range 0.9–1.2. The value of K_1 depended strongly on both the area and the shape of the constriction, but this linear contribution to $p_1 - p_2$, although not negligible, was relatively small (<20%) for a severe constriction ($A = 0.11$) at Reynolds numbers of the order of 1000. In some subsequent experiments on constrictions made by boring small cylindrical holes through cylindrical plugs, Seeley & Young (1976) found rather higher values of K_2 (1.3–1.8), but the earlier, smoothly varying constrictions are expected to be more applicable here. We therefore retain (6.35) and (6.36*a*), but we shall subsequently permit the incorporation of a linear term into the upstream head loss.

At times when the tube is distended, with $A \geq 1$, (6.36a) is inappropriate, because the flow would not be separated. Then we may assume negligible head loss, so that (6.35) can still be used, but with

$$f(A) = \frac{1}{2}(1/A^2 - 1) \leq 0, \quad \text{if } A \geq 1, u_2 > 0. \quad (6.36b)$$

Finally, it is possible that during large-amplitude oscillations, the flow through the constriction might briefly reverse its direction (this has been observed by Dr C. D. Bertram, personal communication). In this case, too, the flow would converge to the constriction, and there would be negligible quasi-steady head loss:

$$f(A) = \frac{1}{2}(1/A^2 - 1) > 0, \quad \text{if } A < 1, u_2 < 0. \quad (6.36c)$$

Momentum/energy equation upstream of the constriction. If the possibility of upstream separation is neglected, as suggested above, then the only quasi-steady head loss between station 1 and the constriction will come about through direct viscous action. The simplest assumption, appropriate for a short length of flexible tube, is to neglect it altogether, and also to neglect the inertia of the fluid in the upstream segment. In that case we have

$$p_1 + \frac{1}{2}u_1^2 - (p + \frac{1}{2}u^2) = 0. \quad (6.37a)$$

However, this is likely to be inappropriate for long flexible segments, for very slight constrictions (where $f(A)$ is small), or for very severe constrictions, when there is a considerable length of collapsed tube with a very small area and a very high resistance. In the latter case especially there will be a significant viscous head loss. To the right-hand side of (6.37a) we therefore add a term $\frac{1}{4}lR(A)u$, where $\frac{1}{4}l$ is an arbitrary representation of the length of the collapsed segment, and $R(A)$ is a dimensionless measure of the resistance per unit length of the collapsed segment with area A .

If the cross-section of the flexible tube upstream of the narrowest point (immediately after which there is a rapid expansion) is assumed to be a slowly varying ellipse, then an appropriate description of the quasi-steady resistance is provided by lubrication theory, from (6.13). When non-dimensionalised as in the present section, this gives

$$R(A) = (4/Re)(\delta + 1/\delta)/A, \quad (6.38)$$

where $Re = \hat{a}_0 \hat{U}_0 / \nu$ is a constant Reynolds number, and δ is the ratio of the minor to the major axis of the ellipse. For a distended tube, with $A > 1$, δ is equal to 1 and (6.38) reduces to Poiseuille's formula, $R(A) = 8/ReA$. When $A < 1$, however, the relation between δ and A must be specified, as in § 6.2. For rubber tubes, the assumption of constant perimeter is appropriate, as given by (6.20), whose right-hand side can be rewritten as $\frac{1}{2}\pi(\delta/A)^{1/2}$. The left-hand side is the complete elliptic integral of the second kind $E(1-\delta^2)$ (Abramowitz & Stegun, 1965, p. 590). Now if $0 \leq \delta \leq 1$, then $1 \leq E(1-\delta^2) \leq 1.57$. Thus a rough, but not unreasonable, approximation in circumstances where δ and A vary widely is to treat E as a constant; here we set $E^2 = 2$, and replace (6.20) by

$$\delta = 8A/\pi^2 \quad \text{when } A < 1. \quad (6.39)$$

When the upstream part of the flexible segment is quite long, the inertia of the fluid in it may not be negligible. We account for it by adding to the right-hand side of (6.37a) another term $l\dot{u}_v$, where u_v is an average fluid speed, which we take, again arbitrarily, to be the speed at the location where the area is A_v (see (6.32)), assumed to be about half-way along the segment. Thus

$$u_v A_v - uA = \frac{1}{2}l\dot{A}_v. \quad (6.40)$$

The final form of (6.37a) is thus

$$p_1 + \frac{1}{2}u_1^2 - (p + \frac{1}{2}u^2) = \frac{1}{4}lR(A)u + l\dot{u}_v. \quad (6.37b)$$

This completes the formulation of the lumped-parameter model. It will be used in three ways: to examine what equilibrium states are possible, to investigate their stability, and to compute the form of the non-linear oscillations that may arise when they are unstable. Whenever numerical values of the dimensionless parameters are required, they will be chosen as far as possible to be comparable with those pertaining to Conrad's (1969) experiments, and will be derived as and when they are needed. Because all parameters cannot be inferred precisely, the results will be only of qualitative value. However, when the model is applied to future experiments, the parameters must be worked out carefully so that quantitative validation may be possible.

6.3.3 *Equilibrium states*

Computation of the equilibrium states should lead to graphs, such as those of fig. 6.3(c) or 6.4(a), of the dimensionless pressure drop across the collapsible segment, $p_1 - p_2$, against the dimensionless flow-rate, Q . For each point on such a curve, therefore, we fix Q and compute the steady value of A that is associated with it. In the steady state u_1 , u_2 and uA are all equal to Q (see (6.30) and (6.31)), and A is computed from the equation obtained by eliminating p and p_2 from (6.27), (6.34) and (6.35), i.e. from

$$R_2 Q - f(A) Q^2 = p_c + P(A), \quad (6.41)$$

where $P(A)$ and $f(A)$ are given by (6.29) and (6.36a or b) respectively. Once A has been computed, p_1 is calculated from (6.37a or b) and P_1 from (6.33).

The roots of (6.41) can be assessed qualitatively from fig. 6.21, where the right-hand side is plotted against A as the continuous curve and there are several plots of the left-hand side, corresponding to various values of Q and of the other parameters. It can be seen that the equation has either one or three roots. It always has at least one root, because (a) $P(A)$ tends to infinity as A tends to infinity, while $f(A)$ tends to $-\frac{1}{2}$, and (b) $P(A)$ (i.e. $-A^{-3/2}$) tends to $-\infty$ more rapidly as A tends to 0 than $-f(A)$ (i.e. $-A^{-1}$). Further, if $R_2 Q > p_c$ there is always one root greater than 1; this state always turns out to be stable, and we can identify it with the state at large flow-rates when the tube is distended. This will correspond to section I of the graph in fig. 6.4: $p_1 - p_2$ will be zero if (6.37a) is used, but not quite zero if (6.37b) is used.

As $R_2 Q$ is slowly reduced below p_c , the equilibrium value of A will fall below 1, i.e. the tube will begin to collapse. The collapse itself will be smooth and gradual if (6.41) has only one root for all Q , as can be seen from the sequence of three broken curves in fig. 6.21. However, if there are three roots when $R_2 Q > p_c$, the collapse will be catastrophic, since the first pair of roots will suddenly cease to exist, and the only possible equilibrium will have a very small value of A . The gradual collapse can conceivably occur quasi-steadily, but the catastrophic collapse cannot possibly do so. The criterion that distinguishes between gradual and catastrophic collapse is whether the slope at $A = 1_-$ of the left-hand side of (6.41) is less than or

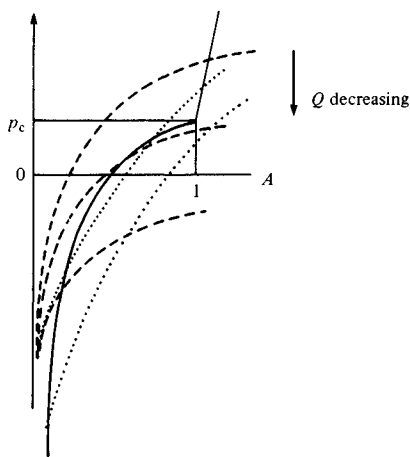


Fig. 6.21. Sketch of the curves representing the two sides of (6.41), plotted against cross-sectional area, A . Continuous curve, right-hand side; broken curves, left-hand side when (6.42) is satisfied, different curves representing different values of Q ; dotted curves, left-hand side when (6.42) is not satisfied.

greater than that of the right-hand side, when $R_2 Q = p_c$. In the case of constant R_2 , this means that the collapse will be gradual if

$$R_2 \geq p_c / (1.5 P_0)^{1/2} \quad (6.42)$$

and catastrophic otherwise. There do not seem to have been any previous theoretical or experimental studies that distinguish between these two modes of collapse, although in their models of forced expiration, Clément *et al.* (1973) considered only catastrophic collapse, while Lambert & Wilson (1972) implicitly considered only gradual collapse. As we shall see, the behaviour of the collapsing tube, as represented for example by the graph of A against t , depends critically on whether (6.42) is satisfied or not.

In order to compute the details of these equilibrium states, we need to assign numerical values to the parameters P_0 , p_c , R_2 and l . A complete survey of all possible values has not yet been undertaken; only values roughly appropriate to Conrad's (1969) experiments have been used. The internal radius of Conrad's uncollapsed tube, \hat{a}_0 , was 0.0063 m, and its length was 0.089 m; we shall take $l = 10$. Conrad employed flow-rates of up to $3 \times 10^{-5} \text{ m}^3 \text{ s}^{-1}$ (see fig. 6.3);

we choose the velocity-scale, \hat{U}_0 , to be 0.15 m s^{-1} , corresponding to a flow-rate of $1.9 \times 10^{-5} \text{ m}^3 \text{ s}^{-1}$, so that the pressure-scale $\rho \hat{U}_0^2$ is 22.5 N m^{-2} ($\rho = 10^3 \text{ kg m}^{-3}$ for water). The Reynolds number, Re , is 860 ($\nu = 1.1 \times 10^{-6} \text{ N m}^{-2} \text{ s}$ for water). The external pressure used for all the experiments of fig. 6.3(c) was 29.5 mmHg, which corresponds to a value of $p_c = 180$; in most computations we have used $p_c = 200$, which tends to increase the maximum values of $p_1 - p_2$ somewhat above those shown in fig. 6.3(c).

We can obtain a rough estimate of P_0 by using the theory of Flaherty *et al.* (1972a), which was translated into the form of a graph of transmural pressure against area by Shapiro (1977). Shapiro's fig. 1, for example, shows that $A = 0.21$ when $\hat{p}_{tm} = -10E(h/\hat{a}_0^3)/12(1 - \sigma^2)$, where E and σ are the Young's modulus and Poisson's ratio of the tube wall and h is its thickness. Conrad (1969) reported that his tubes had $E \approx 1.6 \times 10^5 \text{ N m}^{-2}$ and $h = 0.93 \text{ mm}$, and rubber has a Poisson's ratio close to 0.5, so that in dimensionless terms $P = -25.4$ when $A = 0.21$. Using (6.29), therefore, we obtain $P_0 = 2.7$. In all computations we have used the slightly stiffer value of 4; this has the effect of diminishing the maximum of the $p_1 - p_2$ versus Q graph.

Finally we must choose $R_2 = \hat{R}_2/\rho \hat{U}_0$. In most calculations this is taken to be a constant for convenience, although most of Conrad's downstream resistance came from an adjustable constriction across which the pressure drop was equal to $k_2 \hat{Q}^2$ plus a constant. This change turns out to have no important effect, and we estimate a suitable value for R_2 from curve 4 of fig. 6.3(b). Taking $\hat{p}_2 = 15 \text{ mmHg}$ at a flow-rate of $10 \text{ cm}^3 \text{ s}^{-1}$ we obtain $R_2 \approx 170$. In fact the values we use below are $R_2 = 150, 75, 50$. Note that the smallest of these values is less than $p_c/(1.5P_0)^{1/2}$ (see (6.42)), while the other two are above it. Also, the smaller R_2 is, the higher we expect the maximum of the $p_1 - p_2$ versus Q curve to be (fig. 6.3(c)).

Results of the equilibrium computations are given in figs. 6.22(a) and (b). The continuous curves are those obtained using the full equation (6.37b), while the broken curves are derived by neglecting viscous resistance in the collapsible segment itself (see (6.37a)). Inclusion of the viscous resistance increases the pressure drop, especially at low flow-rates, where the concave nature of the broken curves is almost converted to the approximately linear form

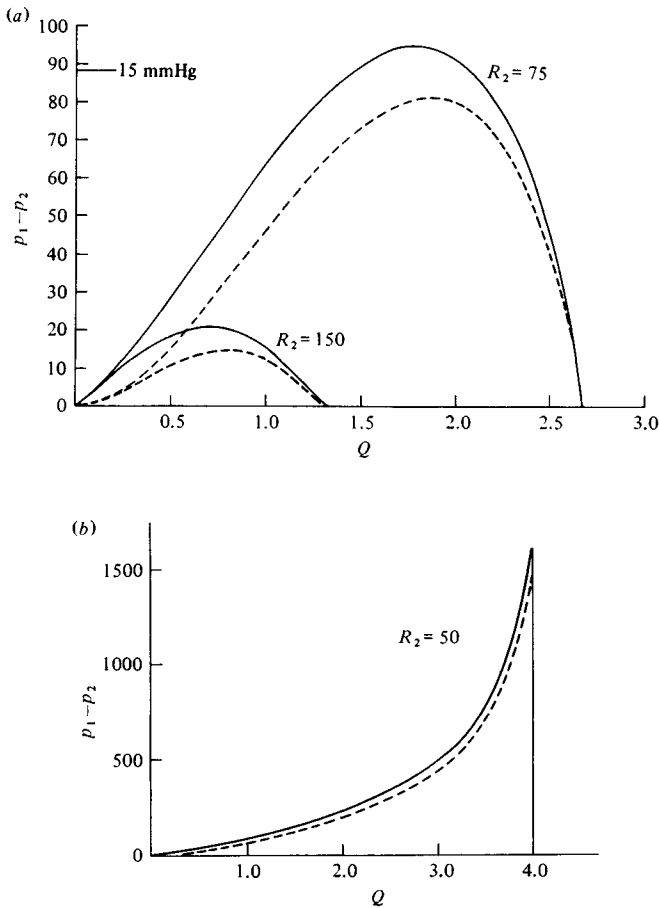


Fig. 6.22. Graphs of $p_1 - p_2$ against Q , as calculated from the lumped-parameter model; $P_0 = 4$, $p_c = 200$, $l = 10$. Continuous curves, $R(A)$ given by (6.38); broken curves, $R(A) = 0$. (a) $R_2 = 75$ and $R_2 = 150$, for which (6.42) is satisfied. (b) $R_2 = 50$, for which (6.42) is not satisfied.

observed experimentally (fig. 6.3(c)). For values of Q greater than p_c/R_2 , the pressure drop across the collapsible segment is, of course, zero when viscous resistance is not incorporated, and turns out to be negligibly small even when it is incorporated. In fact, the continuous curves in fig. 6.22(a), representing the cases of gradual collapse ($R_2 = 150, 75$), bear a close qualitative resemblance to the experimental curves, including the effect of reducing the down-

stream resistance, which is to increase the value of the maximum pressure drop and to extend the range of flow-rates for which collapse occurs. An exactly similar effect is obtained by increasing the chamber pressure, p_c , as is observed experimentally and as is easily predictable from (6.41). We might note here that there is no qualitative difference if the downstream resistance is made non-linear by writing $k_2 Q$ for R_2 , except that the broken curves become even more concave at small flow-rates.

For quantitative comparison with experiment, the results in fig. 6.22(a) must be converted into dimensional terms. The case $R_2 = 150$, chosen to correspond roughly with curve 4 of fig. 6.3, has a maximum value of $p_1 - p_2$ of about 20, which represents 450 N m^{-2} or 3.4 mmHg; this is much less than the value of about 22 mmHg recorded in fig. 6.3(c). Furthermore, the value of Q at which the tube becomes circular, about 1.33, corresponds to a flow-rate of about $25 \text{ cm}^3 \text{ s}^{-1}$, significantly bigger than the observed value of $15 \text{ cm}^3 \text{ s}^{-1}$. The latter discrepancy is reduced by taking the more appropriate values of p_c and R_2 derived above (180 and 170 respectively) when the critical flow-rate is reduced to $20 \text{ cm}^3 \text{ s}^{-1}$, but that reduces the maximum value of $p_1 - p_2$ still further. Even when the smaller value of 2.7 is used for P_0 , the maximum value of $p_1 - p_2$ is restored to only about 23. It is only when P_0 is reduced to the low value of 1.0 that the maximum value of $p_1 - p_2$ becomes comparable with the observations: $(p_1 - p_2)_{\max} = 127 \approx 21 \text{ mmHg}$ (fig. 6.23).† If R_2 is reduced to 75, then the maximum pressure drop becomes comparable with those observed with the original values of P_0 and p_c (4 and 200 respectively), but then the range of flow-rates for which collapse occurs extends far beyond those observed (fig. 6.22(a)). Thus *close* quantitative agreement with Conrad's experiments can be achieved only by adjusting the parameters away from the values chosen *a priori*; this may be because the parameters were not correctly chosen originally, but is equally likely to stem from the crudeness of the present model. The good qualitative

† After this book had gone to press, Mr Conrad informed me that there was a misprint in his 1969 paper and that the actual thickness of the tube wall was much less than the value quoted. Hence P_0 should be considerably smaller than 1, and agreement between these calculations and Conrad's experiments is unlikely to be quantitatively very good.

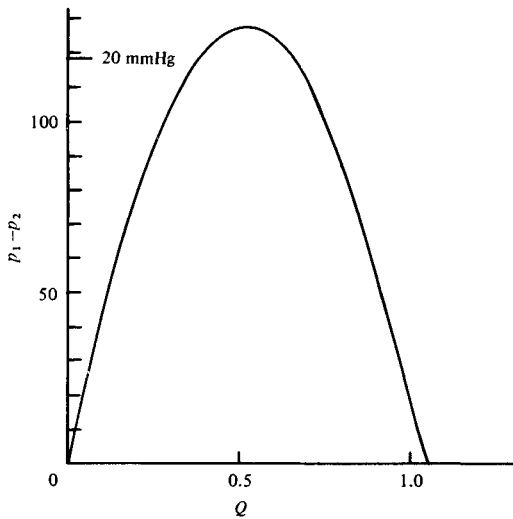


Fig. 6.23. Graph of $p_1 - p_2$ against Q , as calculated from the lumped-parameter model; $P_0 = 1$, $p_c = 180$, $R_2 = 170$, $l = 10$.

agreement, on the other hand, makes one reasonably confident that the chief physical mechanisms underlying the equilibrium states have been incorporated in the model, at least when it predicts gradual collapse.

However, a completely different picture is presented when R_2 is sufficiently low for catastrophic collapse to be predicted (fig. 6.22(b)). Here the shape of the $p_1 - p_2$ versus Q graph is quite different, and the maximum value of $p_1 - p_2$ is far greater, representing a dimensional pressure drop of 270 mmHg. Furthermore, although the equilibrium value of A is an increasing function of Q for small Q , as in the case of gradual collapse, in this case A starts to decrease again when Q exceeds 2.6. Nothing like this has ever been reported experimentally, which suggests strongly that the predicted equilibrium is unstable and that oscillations should be seen.

6.3.4 Stability and oscillations

The stability of an equilibrium and whether or not oscillations develop when it is unstable depend on what quantity is held

constant as the equilibrium is perturbed. In an experiment the most natural such quantity is P_1 , the overall driving pressure head, while another possibility is u_1 , the flow-rate through the upstream rigid segment; the two would be equivalent if the upstream resistance R_1 were effectively infinite. For most of the present calculations we take P_1 to be constant.

To examine the stability of an equilibrium we denote the equilibrium values of all variables by the suffix zero, and suppose that they are all subjected to a small perturbation with exponential time variation. Thus we set

$$A = A_0 + a' e^{\sigma t}, \quad u = u_0 + u' e^{\sigma t}, \quad u_2 = Q_0 + u'_2 e^{\sigma t}$$

etc. and substitute into the governing equations (6.27) and (6.29)–(6.40), neglecting non-linear terms in the perturbation amplitudes a' , u' etc. These perturbation amplitudes are then eliminated from the equations, and the result is a cubic equation for σ . If any root of this equation has positive real part, then the equilibrium is unstable. The cubic obtained when the viscous pressure drop in the collapsible segment is not ignored (i.e. when (6.37*b*) is used, not (6.37*a*)), and R_1 and R_2 are taken to be constant, is

$$C_3 \sigma^3 + C_2 \sigma^2 + C_1 \sigma + C_0 = 0, \quad (6.43)$$

where the coefficients are given by

$$\begin{aligned} C_3 &= \frac{1}{2} l I_2 [I_1 + l / (1 + A_0)], \\ C_2 &= \frac{1}{2} l I_2 [R_1 - Q_0 - 4 \dot{Q}_0 / (1 + A_0)^2] \\ &\quad + \frac{1}{2} l [I_1 + l / (1 + A_0)] (R_2 - 2 Q_0 f_0), \\ C_1 &= \frac{1}{2} l (R_2 - 2 Q_0 f_0) [R_1 - Q_0 - 4 \dot{Q}_0 / (1 + A_0)^2] \\ &\quad + I_2 [P'_0 - u_0^2 / A_0 + \frac{1}{4} l u_0 (R'_0 - R_0 / A_0)] \\ &\quad + [I_1 + 2 l / (1 + A_0)] (Q_0^2 f'_0 + P'_0), \\ C_0 &= (R_2 - 2 Q_0 f_0) [P'_0 - u_0^2 / A_0 + \frac{1}{4} l u_0 (R'_0 - R_0 / A_0)] \\ &\quad + (R_1 - Q_0 + u_0 / A_0 + \frac{1}{4} l R_0 / A_0) (Q_0^2 f'_0 + P'_0). \end{aligned}$$

In these equations $f_0, f'_0, P'_0, R_0, R'_0$ represent the relevant functions evaluated at $A = A_0$: $f_0 = f(A_0)$, $P'_0 = P'(A_0)$, etc.

Whether or not the roots of a cubic have positive real part can be determined from *Routh's criterion*, which is very clearly expounded

by Porter (1967). In the case when C_3 is positive, as here, this can be stated as follows:

- (a) If $C_0 < 0$, the equation has at least one positive real root; that is, the instability can be classed as an exponential instability, in which the disturbance grows monotonically, without oscillation.
- (b) If $C_0 > 0$ and either $C_2 < 0$ or $C_2C_1 - C_3C_0 < 0$ (or both) the equation has two roots with positive real part; these roots may be either real or complex. If they are complex, the instability will be in the form of a growing oscillation. If all the C s are positive, and $C_2C_1 - C_3C_0 < 0$, then the two roots with positive real part *must* be complex.

It can be shown after a little algebra that

$$C_0 = (P'_0 + Q^2 f'_0) dP_1/dQ,$$

where dP_1/dQ is the rate at which the overall driving pressure increases with the flow-rate, i.e. the *overall* resistance of the system. Furthermore, the factor $P'_0 + Q^2 f'_0$ is positive at all the equilibrium areas A_0 for which the slope of the continuous curve in fig. 6.21 exceeds that of the broken or dotted curve, i.e. for all equilibria except the middle one when there are three. This middle equilibrium has $C_0 < 0$, and is therefore unstable wherever $dP_1/dQ > 0$, which is the normal situation. The other equilibria, however, have $C_0 < 0$ if and only if $dP_1/dQ < 0$, i.e. exponential instability will result whenever the resistance of the system is negative. This is a familiar result from electrical circuit theory; attention has been drawn to it by both Conrad (1969) and Griffiths (1975). However, this instability does not normally lead to oscillation. At values of P_1 for which $dP_1/dQ < 0$ there are three possible equilibrium values of Q . Although the middle one is unstable, the system will tend to one of the others if that is stable, and the one with $A > 1$ always is stable.

The use of Routh's criterion, however, demonstrates that instability may arise when the overall resistance is not negative, a result that does not previously seem to have been noticed in the present context. This instability must lead to oscillation because there is no other equilibrium at the given value of P_1 . The coefficients of (6.43) are too complicated for criteria based on the

system's parameters to become immediately obvious, but numerical calculation of the roots of (6.43) confirms the possibility of such an instability for realistic parameter values.

Before the roots of (6.43) can be computed, it is necessary to choose values for the additional parameters, I_2 , I_1 and R_2 . If the pressure difference required to give an average acceleration $d\hat{u}_2/d\hat{t}$ to the fluid in the downstream rigid tube is $\hat{I}_2 d\hat{u}_2/d\hat{t}$, then $I_2 = \hat{I}_2/\rho\hat{a}_0$. We estimate \hat{I}_2 as the mass of fluid in the downstream segment divided by its cross-sectional area, so that $I_2 = \hat{I}_2/\hat{a}_0$, where \hat{I}_2 is the length of the segment. Conrad (1969) did not report the value of \hat{I}_2 , but his diagrams suggest that it was about $2\frac{1}{2}$ times the length of the collapsible segment. We therefore choose $I_2 = 25$. Conrad also did not report any details of the upstream rigid segment, because his rather simplified theory did not reveal its possible importance. In accordance with what would be the case if both rigid segments were long and straight, we have chosen to keep the ratios I_1/I_2 and R_1/R_2 equal to each other, at a value β , say. We have then chosen to examine three different values of β , equal to 1.5, 1.0 and 0.5.

The results of the stability calculation, for the equilibrium states represented by the continuous curves in figs. 6.22 and 6.23, are as follows.

- (a) $P_0 = 4$, $p_c = 200$, $R_2 = 150$ (the lower curve in fig. 6.22(a)). This case is stable for all Q and for all three values of β .
- (b) $P_0 = 4$, $p_c = 200$, $R_2 = 75$ (the upper curve in fig. 6.22(a)), and $\beta = 1.5$ so that $R_1 = 1.5R_2$. There is a 'negative-resistance' (non-oscillatory) instability for a small range of flow-rates just below the value above which the tube remains circular: $2.51 < Q < 2.67$. There are no other instabilities. This result agrees with the experimental evidence that instability arises only for sufficiently small values of R_2 .
- (c) The same values of P_0 , p_c , R_2 but smaller values of β ($= 1.0$, 0.5). In each case the negative-resistance instability arises for a comparable range of flow-rates: $2.43 < Q < 2.67$ for $\beta = 1.0$ and $2.32 < Q < 2.67$ for $\beta = 0.5$. However another, oscillatory instability becomes manifest for a range of smaller flow-rates, owing to the fact that $C_2C_1 - C_3C_0 < 0$ ($C_2 > 0$). The range of

flow-rates is $1.39 < Q < 1.90$ for $\beta = 1.0$ and $0.77 < Q < 2.32$ for $\beta = 0.5$, which in each case overlaps the rising part of the $p_1 - p_2$ versus Q curve in fig. 6.22(a). Neither Conrad (1969) nor Katz *et al.* (1969) observed oscillations in such circumstances, no doubt because the values of R_1 applicable to their experiments were too large. This prediction of an instability that does not depend on negative resistance suggests an interesting avenue of future experimental research.

- (d) $P_0 = 4$, $p_c = 200$, $R_2 = 50$ (fig. 6.22(b)). This is the case of catastrophic collapse according to the equilibrium calculation. Here the overall resistance increases with Q for all Q up to 4, at which value it falls dramatically but above which there is a stable equilibrium with $A > 1$. Nevertheless, even with $\beta = 1.5$, the equilibria in most of the range $0 < Q < 4$ are unstable, with $C_2 C_1 - C_3 C_0 < 0$, $C_2 > 0$. Only the smallest flow-rates, $0 < Q < 0.62$, lead to stable equilibrium. This was foreseen above, and would explain why graphs like fig. 6.22(b) are not obtained in practice.
- (e) $P_0 = 1$, $p_c = 180$, $R_2 = 170$ (fig. 6.23). This is the case for which the equilibrium predictions have the closest quantitative agreement with Conrad's experiments. No instability is predicted for $\beta = 1.5$, but a negative-resistance, and hence non-oscillatory, instability is predicted for $\beta = 1.0$, when Q lies in the range $0.88 < Q < 1.05$. (This range would coincide closely with the gap in curve 4 of fig. 6.3(c) if the scale for Q were adjusted to make the critical flow-rates for collapse ($Q = p_c/R_2$) coincide. As it is, the predicted p_c/R_2 corresponds to a flow-rate of $20 \text{ cm}^3 \text{ s}^{-1}$, not $15 \text{ cm}^3 \text{ s}^{-1}$ as measured.)
- (f) Finally we consider what happens if either or both of R_1 and I_1 are very large: this would be one way, in practice, of ensuring that the upstream velocity, u_1 , remained constant. In this case the coefficients in (6.43) are given approximately by

$$\begin{aligned} C_3 &= \frac{1}{2} I_1 I_2, & C_2 &= \frac{1}{2} l (I_2 R_1 + I_1 R_2 - 2 I_1 Q_0 f_0), \\ C_1 &= \frac{1}{2} l R_1 (R_2 - 2 Q_0 f_0) + I_1 (Q_0^2 f_0' + P_0'), \\ C_0 &= R_1 (Q_0^2 f_0' + P_0'). \end{aligned}$$

We have already seen that $Q_0^2 f_0' + P_0' > 0$ for all equilibria of

interest, so Routh's criterion predicts instability only if either $C_2 < 0$ or $C_2C_1 - C_3C_0 < 0$, i.e. only if

$$R_2 - 2Q_0f_0 < 0. \quad (6.44)$$

This is the same condition that we would have obtained by setting u_1 equal to a constant at the outset of the stability analysis. It can also be regarded as a negative-resistance instability in that

$$R_2 - 2Q_0f_0 = dp_0/dQ_0,$$

so that instability is predicted if the net resistance of those parts of the system downstream of the constriction is negative. Examination of the equilibrium equation (6.41) shows that (6.44) is also equivalent to the condition $dA_0/dQ_0 < 0$, and the only one of the examples computed above that satisfies this is the case of catastrophic collapse (fig. 6.22(b)) for $2.6 < Q < 4.0$. The examples plotted in figs. 6.22(a) and 6.23 would be stable if u_1 were held constant. However, there is no *a priori* reason why this instability should be associated only with catastrophic collapse.

The above results show that the values of the resistances and inertances of the rigid tubes have a strong effect on whether the flows are unstable and on what type of instability is predicted. It is also likely that they will influence the non-linear motion that develops after instability: as reported by both Conrad (1969) and Ur & Gordon (1970), a range of oscillation frequencies can be obtained by adjusting the parameters. On the other hand, the *shape* of the oscillations, as indicated by the graphs of A and Q against t , for example, will be dominated by the non-linearities and are unlikely to be greatly affected by the rigid-tube parameters.

A few preliminary examples, computed by Dr C. D. Bertram, are shown in figs. 6.24–6.26. The standard parameters, $P_0 = 4$, $p_c = 200$, $l = 10$, are the same in each case, while R_2 and β are different. The plots in parts (a) are of A against t , while those of parts (b) are of u_2 against t . Fig. 6.24 shows the oscillations that develop in a case of gradual collapse when the equilibrium suffers an oscillatory instability ($R_2 = 75$, $\beta = 0.5$, $P_1 = 259$ corresponding to $Q = 1.5$ in fig. 6.22(a)), while fig. 6.25 shows the corresponding graphs for a

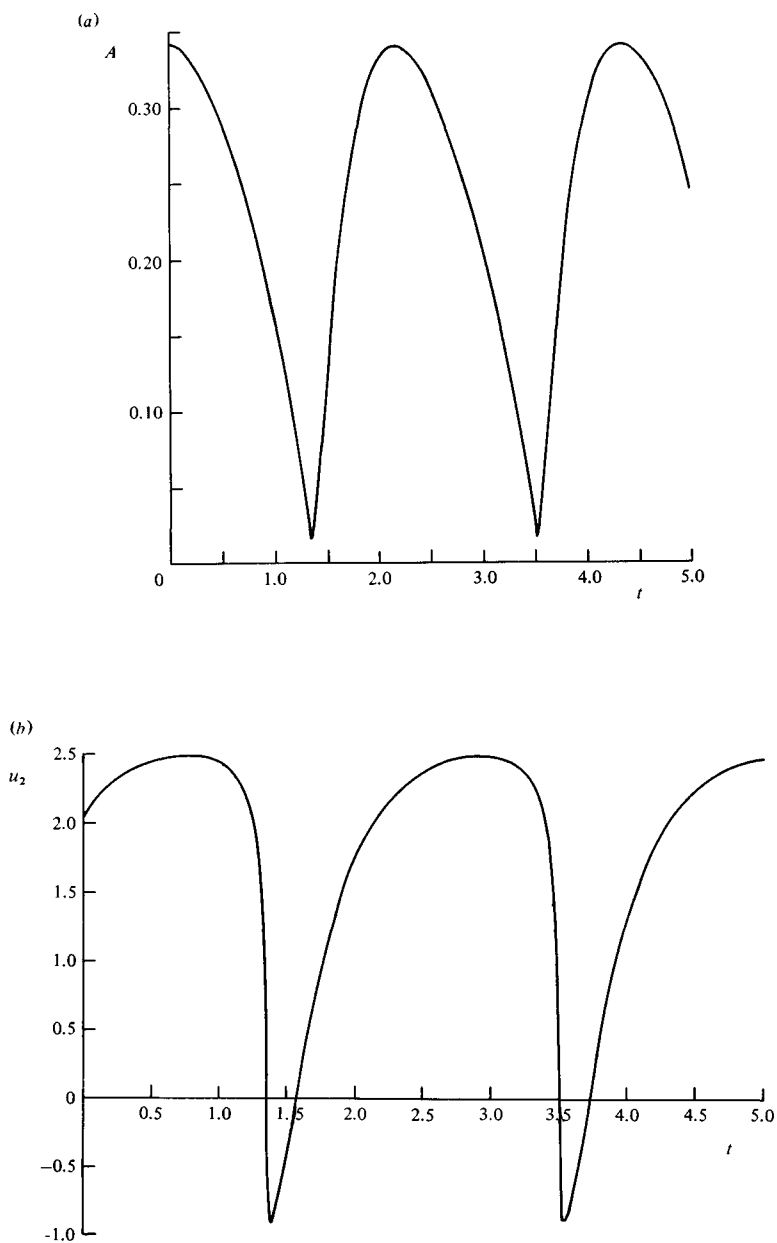


Fig. 6.24. Steady state oscillations, represented by graphs of (a) A against t and (b) u_2 against t . $R_2 = 75$, $\beta = 0.5$, $P_1 = 259$.

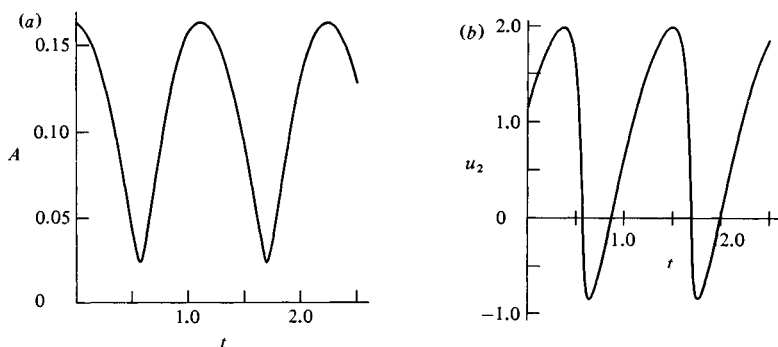


Fig. 6.25. As fig. 6.24, with $R_2 = 50$, $\beta = 1.5$, $P_1 = 209$.

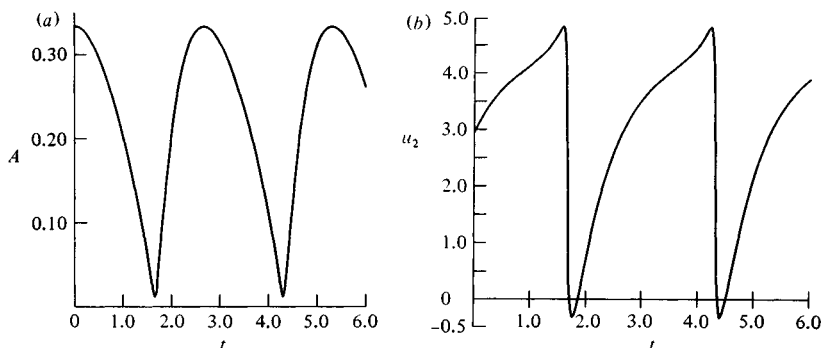


Fig. 6.26. As fig. 6.24, with $R_2 = 50$, $u_1 = 3$ (fixed).

case of catastrophic collapse ($R_2 = 50$, $\beta = 1.5$, $P_1 = 209$ corresponding to $Q = 1.0$ in fig. 6.22(b)). The oscillations have different amplitudes and frequencies, and somewhat different shapes, although in each case the tube tends to remain open, with a relatively high velocity through it, for a longer fraction of the cycle than it remains almost closed (this is especially true for the case depicted in fig. 6.24). Note too that in each case there is a brief period of downstream flow reversal shortly after the time at which the area of the constriction is narrowest.

Fig. 6.26 shows the corresponding curves for an unstable case in which u_1 is held constant ($R_2 = 50$, $u_1 = 3$). Here the area curves do not look very different, but the downstream velocity varies in a quite

different manner. The detailed mechanics have not yet been investigated, but the difference is no doubt associated with the fact that this is a case of exponential, not oscillatory, instability. We may note that, as expected, the negative-resistance instabilities for cases with P_1 fixed do not in this model lead to oscillations.

Finally, the difference between gradual and catastrophic collapse is investigated by allowing P_1 to fall gradually from a large value at which the tube is uncollapsed, and stable, to one for which it is collapsed. Fig. 6.27 shows the variation of A with t in three different cases; in each case $dP_1/dt = -0.1$. The first is a case of gradual collapse, where no instability is predicted at any stage, and no oscillations are observed (fig. 6.27(a)). The second is also a case of gradual collapse, but one in which negative resistance, and hence instability, is predicted for a small range of flow-rates; this manifests itself as a damped oscillation as the collapse proceeds (fig. 6.27(b)). Finally, we show in fig. 6.27(c) a case of catastrophic collapse, with $R_2 = 50$. In this case our rather elementary computer programme broke down for values of R_1 comparable with those used in the other cases, because A was predicted to fall rapidly to a value as small as the accumulated numerical errors. The computations were therefore carried out for a very large value of R_1 ($\beta = 10^6$), which constrains u_1 to be approximately proportional to P_1 , and the quasi-steady-state oscillations that develop are comparable with those for fixed u_1 shown in fig. 6.26.

Although these results are only preliminary, they do indicate that the present crude, lumped-parameter model is capable of describing a wealth of physical phenomena, not all of which have yet been fully understood or realised experimentally. There is clearly scope for a great deal of further work, both theoretical and experimental, even without taking into account those aspects of unsteady flow in collapsible tubes that cannot be described by a lumped model.

6.4 Other mechanisms of instability

The above analysis has shown that certain mechanisms by which oscillations in collapsible tubes are excited can be described by a lumped-parameter model. In this section we examine other mechanisms that cannot be so described. The discussion is based on

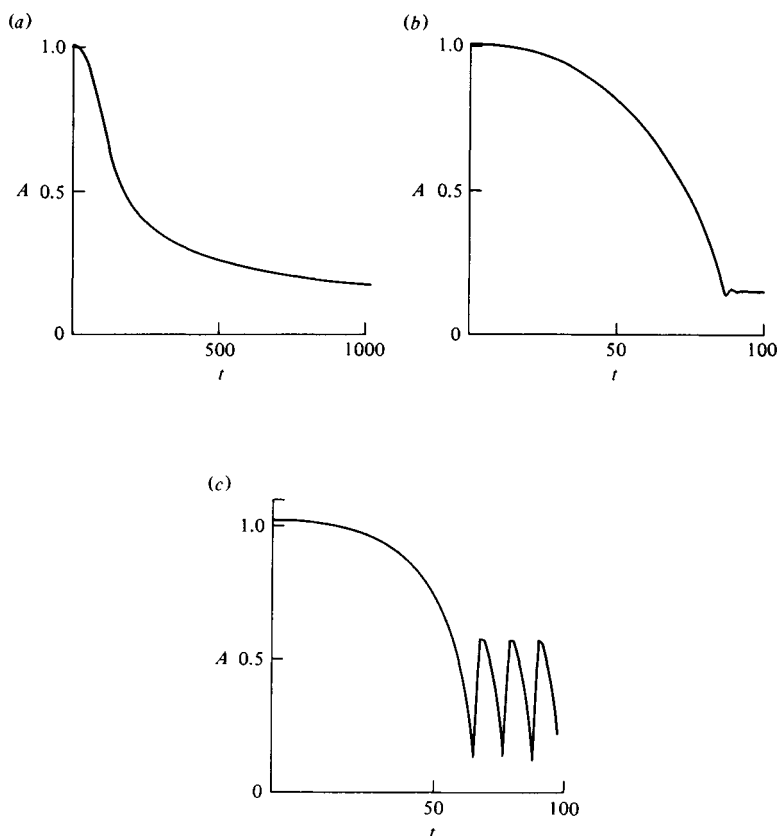


Fig. 6.27. Graphs of A against t for gradually falling values of P_1 . (a) $R_2 = 150$, $\beta = 1.5$: gradual collapse, stable. (b) $R_2 = 75$, $\beta = 1.5$: gradual collapse, unstable. (c) $R_2 = 50$, $\beta = 10^6$: catastrophic collapse, unstable.

the equations governing approximately one-dimensional flow in a slowly varying collapsible tube, as set out in chapter 2. We let $A(x, t)$, $p(x, t)$ and $u(x, t)$ be the dimensionless cross-sectional area, pressure and velocity in the segment of tube upstream of the narrowest point. (Downstream of that point the tube area opens out very rapidly again as it joins to the downstream rigid tube and the one-dimensional model proposed here will break down.) The relevant equations are then those of elasticity

$$p - p_c = P(A), \quad (6.45)$$

of continuity

$$A_t + (uA)_x = 0, \quad (6.46)$$

and of momentum

$$u_t + uu_x = -p_x - R(A)u. \quad (6.47)$$

The last term in (6.47) represents the viscous force, averaged across a cross-section of the tube; a more general form could be used, but we have assumed that the velocity profile is quasi-steady and quasi-parallel so that this term is linear in u , and $R(A)$ can be deduced from lubrication theory. If we further assume that the cross-section of the tube remains elliptical, then (6.38) can be used for $R(A)$; however, the only properties of $R(A)$ that are important here are that it is positive and that it increases more rapidly than $1/A$ as A decreases.

There are a number of other factors that may be important in other experiments. These include variation of external pressure, p_c , with x , a longitudinal component of body force such as gravity (which is actually equivalent to a variation of p_c with x), and variation with x of the elastic properties of the tube, so that (6.45) is replaced by

$$p - p_c = P(A, x).$$

The equilibrium states of such more general systems have been exhaustively studied by Shapiro (1977), and a variety of steady and unsteady phenomena associated with them have been described by Griffiths (1971, 1975). However, the main points can be made with reference to the simple set of equations (6.45)–(6.47).

In looking for equilibrium conditions we set the time derivatives equal to zero and eliminate p to obtain

$$A_x/A = -R(A)u/(c^2 - u^2), \quad (6.48)$$

where

$$c = [AP'(A)]^{1/2} \quad (6.49)$$

is the dimensionless speed of infinitesimal pressure waves along the tube when its cross-sectional area is A (cf. (2.4)). We shall describe flows for which $u < c$ or $u > c$ as subcritical or supercritical respectively, by analogy with free surface liquid flow in a uniform channel

(Shapiro (1977) thoroughly examined the analogies between flow in collapsible tubes and both channel flow and compressible gas flow in rigid tubes). If we suppose that the flow is subcritical at the point where it enters the collapsible segment, then (6.48) shows that A is a decreasing function of x . Now the flow-rate Q is constant, so $u = Q/A$ must be an increasing function of x . For the model chosen here, in which $P(A)$ is given by (6.29) with $A_c = 1$, c is given by

$$\begin{aligned} c^2 &= 10P_0A, & A > 1, \\ &= 1.5P_0/A^{3/2}, & A < 1, \end{aligned} \quad (6.50)$$

so for $A < 1$, c is also an increasing function of x , but it does not increase as rapidly as u . Thus if the tube is long enough, a point will eventually be reached at which $u = c$. At this point $-A_x$ is predicted to be infinite, so the model must have broken down before then; we conclude that a steady flow with the prescribed value of Q is impossible. This is the phenomenon of 'choking' familiar from gas dynamics.

Suppose that the pressure far upstream, P_1 , is gradually raised from a value at which steady, subcritical flow is possible everywhere upstream of the narrowest point. As P_1 increases, Q will also increase until *either* instability occurs according to the lumped model, and we suppose that this does not happen, *or* the flow becomes critical at the narrowest point. For higher values of P_1 the steady flow cannot be maintained and oscillations must ensue. There is no possibility, as there sometimes is in channel flow or gas dynamics, of a continuous passage through the critical point with a hydraulic jump or shock (or 'elastic jump': Dawson & Elliott, 1977) downstream, because the numerator of (6.48) cannot be made to go to zero when the denominator does. As P_1 is raised above the critical value, the flow will remain almost critical at the narrowest point, and a pressure wave will propagate upstream to reduce the incoming flow-rate. However, since P_1 is held fixed, this will be reflected and the process will constantly repeat itself in an oscillatory manner. No complete model of such oscillations has yet been constructed, although Reyn (1974) has done some preliminary calculations on a model that neglects all energy dissipation except that occurring in 'shocks' as and when they develop.

An estimate of whether choking will occur in a particular case can be made if we assume that the lumped-parameter model is valid downstream of the narrowest point; the area at that point will then be given in terms of Q by (6.41). Of the examples computed above, choking occurs in some cases that were predicted to be stable as well as some unstable cases (e.g. $R_2 = 75$, $Q = 1.5$ from fig. 6.22(a), which is stable if $\beta = 1.5$ but unstable if $\beta = 0.5$ or 1.0), and does not occur in others, including cases that were predicted to be unstable (e.g. $R_2 = 75$, $Q = 1.0$, $\beta = 0.5$; or $R_2 = 50$, $Q = 1.3$, $\beta = 1.5$). Choking is not found at any flow-rate when $R_2 = 150$. We conclude that oscillations in a given experiment may involve either choking or a lumped-model instability or both; Conrad's (1969) experiments are particularly difficult to interpret in this context.

Finally, let us assume that choking does not occur, and that upstream of the constriction the equations (6.45)–(6.47) have equilibrium solutions $A = A_0(x)$, $p = p_0(x)$, $u = u_0(x)$. Can these be unstable by a mechanism that is not included in the lumped model? In order to investigate this, we suppose that the equilibrium solutions are sufficiently slowly varying with x that, at each x , they may be regarded as uniform for the purpose of a stability analysis. We then set

$$A = A_0 + a'(x, t)$$

with similar expressions for p and u , substitute into (6.45)–(6.47), linearise, and eliminate p' and u' . The resulting equation for a' is then

$$\begin{aligned} & [\partial/\partial t + (u_0 + c_0) \partial/\partial x][\partial/\partial t + (u_0 - c_0) \partial/\partial x]a' \\ & + R(A_0)(\partial/\partial t + c_1 \partial/\partial x)a' = 0, \end{aligned} \quad (6.51)$$

where c_0 is the wave speed, from (6.49), evaluated at area A_0 , and

$$c_1 = u_0[1 - A_0 R'(A_0)/R(A_0)]. \quad (6.52)$$

Equation (6.51) is the equation that describes roll-waves in open channels (see Dressler, 1949; and Whitham, 1974, p. 85). It follows immediately that the equilibrium flow is stable if and only if

$$u_0 - c_0 < c_1 < u_0 + c_0.$$

In our case $u_0 < c_0$, because choking is assumed not to occur, so the first inequality is identically satisfied. The second inequality then

predicts that instability will occur if

$$u_0/c_0 > -R(A_0)/A_0 R'(A_0); \quad (6.53)$$

the right-hand side of this is positive because R is a decreasing function of A .

If the tube cross-section remained circular at all times, then $R \propto 1/A$ and the right-hand side of (6.53) would be equal to 1. In that case instability would be predicted to set in at the same fluid velocity as choking; any velocity lower than c_0 would be stable. However, in our case R increases more rapidly than $1/A$ as A decreases, so the right-hand side of (6.53) is less than 1, and instability by this roll-wave mechanism will occur at a velocity less than the wave speed. Thus choking will never be the sole cause of oscillation; roll-wave instability must occur first.

If the cross-sectional area is very small, then (6.38) and (6.39) show that $R \propto 1/A^2$, with the consequence that the critical velocity is one-half of the wave speed:

$$u_{\text{crit}} = \frac{1}{2}c_0 = 0.61P_0^{1/2}A_0^{-3/2}.$$

Some of the maximum equilibrium velocities calculated from the above lumped model exceed this value (e.g. the unchoked case $R_2 = 75$, $Q = 1.0$ from fig. 6.22(a), which is stable according to the lumped model if $\beta = 1.5$ but not if $\beta = 0.5$) while others, including cases that are unstable by the lumped mechanism, do not (e.g. $R_2 = 50$, $Q = 0.65$, $\beta = 1.5$ from fig. 6.22(b)). Thus there certainly will be circumstances in which the roll-wave instability is the dominant cause of oscillation, and others in which the lumped-parameter mechanism dominates.

As we have already remarked, roll-wave instability will always occur at a lower velocity than choking, and thus, in the particular experiment modelled here, should be regarded as a more important source of unsteady behaviour. The only other well-known example of this kind of instability, roll-waves themselves in channel flow, is not widely observed and not regarded as very important. This is doubtless because in that case they occur only at supercritical speeds, and supercritical channel flows more often break down through single hydraulic jumps or bores.

The next stage of this theoretical work must be to combine the lumped-parameter model for flow downstream of the constriction with the quasi-one-dimensional analysis of this section for flow upstream of it. This will result in a non-linear set of hyperbolic partial differential equations that will have to be solved numerically, although one hopes that the above discussion will provide a useful framework. Other fundamental physical effects that should be incorporated into the model as soon as a clear mathematical description of them can be formulated are the intermittent flow separation and energy loss at an oscillating constriction, and the effects on the tube pressure–area law of longitudinal curvature and longitudinal tension in the wall. Careful experiments must also be done to test all the predictions of the present models and their successors; in particular, the model parameters must be recorded sufficiently accurately that it is at last possible to distinguish between the different mechanisms of instability and of oscillation. Finally, of course, a fuller understanding of the mechanics of collapsible tubes will enable us to make more confident interpretations of physiological phenomena such as flow limitation in forced expiration, venous return, and Korotkoff sounds.